

Article

# A Modified Surface Energy Balance to Estimate Crop Transpiration and Soil Evaporation in Micro-Irrigated Orchards

Camilo Souto <sup>1,2</sup>, Octavio Lagos <sup>1,2,\*</sup>, Eduardo Holzapfel <sup>1,2</sup>, Mahesh Lal Maskey <sup>3</sup>, Lynn Wunderlich <sup>4</sup>, Kristen Shapiro <sup>3</sup>, Giulia Marino <sup>3</sup>, Richard Snyder <sup>3</sup> and Daniele Zaccaria <sup>3</sup>

<sup>1</sup> Departamento de Recursos Hídricos, Facultad de Ingeniería Agrícola, Universidad de Concepción, Chillán 3812120, Chile

<sup>2</sup> Centro de Recursos Hídricos para la Agricultura y Minería (CRHIAM), Universidad de Concepción, Chillán 3812120, Chile

<sup>3</sup> Department of Land, Air and Water Resources, University of California, Davis, CA 95616, USA

<sup>4</sup> University of California Cooperative Extension, Central Sierra Region, 311 Fair Lane, Placerville, CA 95667, USA

\* Correspondence: octaviolagos@udec.cl

Received: 14 June 2019; Accepted: 19 August 2019; Published: 22 August 2019



**Abstract:** A surface energy balance model was conceived to estimate crop transpiration and soil evaporation in orchards and vineyards where the floor is partially wetted by micro-irrigation systems. The proposed surface energy balance model for partial wetting (SEB-PW) builds upon previous multiple-layer modelling approaches to estimate the latent, sensible, and soil heat fluxes, while partitioning the total evapotranspiration ( $ET$ ) into dry and wet soil evaporation ( $\lambda E_{soil}$ ) and crop transpiration ( $T$ ). The model estimates the energy balance and flux resistances for the evaporation from dry and wet soil areas below the canopy, evaporation from dry and wet soil areas between plant rows, crop transpiration, and total crop  $ET$ . This article describes the model development, sensitivity analysis and a preliminary model evaluation. The evaluation shows that simulated hourly  $ET$  values have a good correlation with field measurements conducted with the surface renewal method and micro-lysimeter measurements in a micro-irrigated winegrape vineyard of Northern California for a range of fractional crop canopy cover conditions. Evaluation showed that hourly  $LE$  estimates had root mean square error ( $RMSE$ ) of  $58.6 \text{ W m}^{-2}$ , mean absolute error ( $MAE$ ) of  $35.6 \text{ W m}^{-2}$ , Nash-Sutcliffe coefficient ( $C_{NS}$ ) of 0.85, and index of agreement ( $d_a$ ) of 0.94. Daily soil evaporation ( $E_s$ ) estimations had  $RMSE$  of  $0.30 \text{ mm d}^{-1}$ ,  $MAE$  of  $0.24 \text{ mm d}^{-1}$ ,  $C_{NS}$  of 0.87, and  $d_a$  of 0.94.  $E_s$  estimation had a coefficient of determination ( $r^2$ ) of 0.95, when compared with the micro-lysimeter measurements, which showed that  $E_s$  can reach values from 28% to 46% of the total  $ET$  after an irrigation event. The proposed SEB-PW model can be used to estimate the effect and significance of soil evaporation from wet and dry soil areas on the total  $ET$ , and to inform water balance studies for optimizing irrigation management. Further evaluation is needed to test the model in other partially wetted orchards and to test the model performance during all growing seasons and for different environmental conditions.

**Keywords:** evapotranspiration; shading percentage; micro-lysimeter; energy balance; micro-irrigation

## 1. Introduction

Evapotranspiration ( $ET$ ) is generally the second largest component of water balance, following precipitation. Researchers and water resource managers require accurate and reliable  $ET$  estimates to understand water availability and distribution for both short and long-term water resource

management [1].  $ET$  is the amount of water lost to the atmosphere, including net water evaporation and the water transferred through the vascular system of the plant into the atmosphere from leaves.  $ET$  estimation is not straightforward due to the natural heterogeneity and complexity of the hydrological processes in catchments. Water managers and growers therefore seek robust methods to quantify  $ET$  and assess the impact of water management and conservation measures, such as to reduced tillage, on  $ET$  during crop growing seasons [2]. Evapotranspiration is an integrated term, composed of the precipitation intercepted by plant canopies, vapor fluxes of plant transpiration, and soil evaporation [3]. Transpiration ( $T$ ) is the process of water movement through the plant xylem, and it is the main component of  $ET$  that impacts the  $ET$ -yield relationship. Depending on the type of irrigation system (e.g., surface irrigation, sprinkler irrigation or micro-irrigation), the soil evaporation ( $\lambda E_{soil}$ ) component during the crop growing season can be a significant component of the total  $ET$  [4]. Crop shadowing and the partial wetting of soil by micro-irrigation systems not only affects the processes of  $\lambda E_{soil}$ , but also several relevant  $ET$ -related parameters, such as net radiation, soil heat flux, aerodynamic, and surface resistances to heat and water vapor fluxes [5].

The soil evaporation from bare soil is commonly described as occurring in two or three stages [6]. Stage I is governed by atmospheric conditions, with  $\lambda E_{soil}$  limited only by the available energy in the upper soil layer and by the vapor gradient between the soil and the atmosphere. During stages II and III,  $\lambda E_{soil}$  becomes primarily a function of the soil water content, soil hydraulic properties, and temperature gradients [7]. To assess the dynamics of the multi-stages of evaporation from bare soil,  $\lambda E_{soil}$  is commonly measured with micro-lysimeters (MLs) [8–11].  $\lambda E_{soil}$  can be determined under circumstances where traditional methods are impractical or impossible and can be measured under conditions of partial cover and partial shading, or in other situations for which the spatial resolution of traditional lysimeters is too large [8]. Yunusa et al. [11] measured soil evaporation with MLs at four locations, and found that, during rainy periods when the entire soil surface was wet, the soil evaporation process accounted for up to 80% of  $ET$  (stage I of  $\lambda E_{soil}$ ), and with no substantial addition of water,  $\lambda E_{soil}$  declined to less than 9% of its original value. The progressive  $\lambda E_{soil}$  decline occurs because, as the near-surface layers of the soil dried out, the unsaturated hydraulic conductivity of the soil also declined. The same authors also found that the dominant component of  $ET$  was  $\lambda E_{soil}$  when the prevailing stage-two process of  $\lambda E_{soil}$  was less and similar at all positions, except when the soil surface was dry.

In  $ET$  modeling, process models of latent heat have progressed through phases over time [2]. Penman [12] developed a model for a layer extending from a reference height to a uniform surface, a concept that has been applied to crops by approximating the canopy as a single surface or big leaf in the Penman–Monteith (P–M) method [13]. Several authors have studied the P–M in agricultural crops [14–16], but only some of them accept that a big leaf is not applicable to all crops. Thus, it is assumed that a big leaf condition can cause large errors in the total  $ET$  estimation in a short-time interval.

Various modeling efforts recognized that sparse vegetation and crops with partial canopy cover may not satisfy the big leaf assumption, and models were developed to predict the transpiration and evaporation separately [2]. Several studies evaluated one of these models, known as the Shuttleworth and Wallace [17] (S-W) model [18–21]. Farahani and Ahuja [18] extended the S-W model to include the effects of crop residues on soil evaporation by adding a partially covered soil area and partitioning evaporation between bare and residue-covered areas. Iritz et al. [22] modified the S-W model to estimate the  $ET$  for a boreal forest. The model was modified in terms of the bulk canopy resistance, the calculation of the aerodynamic resistance, and the addition of a two-layer soil module, which enabled the estimation of a soil surface resistance, depending on the wetness of the soil top. Odhiambo and Irmak [23] evaluated the applicability of the extended S-W model for estimating and partitioning  $ET$  in a subsurface drip-irrigated soybean field with a partial residue cover, and compared the S-W model with a Bowen Ratio Energy Balance (BREB) system. They integrated an approach to calculate the bulk stomatal resistance as a function of the soil water content ( $\theta$ ) to allow for the simulation of  $T$  over a range of  $\theta$  values. In general, the model performed well in tracking the trends and magnitude

of  $ET$  measured with the BREB system. Ortega–Fariás and López–Olivari [24] validated a two-layer model to estimate latent heat flux and  $ET$  in a drip-irrigated olive orchard. This study indicated that the two-layer model overestimated the latent heat flux and  $ET$  by about 2% and 6%, respectively, and that the model was very sensitive to errors in the measurements of stomatal conductance. However, the main errors did not significantly affect the overall performance of the two-layer model.

In the 1980s, a more complete surface energy balance model, including the estimation of soil heat flux, was presented by Choudhury and Monteith [25] (Ch-Mon). They developed a four-layer model for the heat budget of homogeneous land surfaces using explicit solutions for the conservation of heat and water vapor in a uniform vegetation and soil system [2]. This model partitioned the available energy into latent heat, sensible heat, and soil heat flux for the canopy/soil system and offered the possibility of including the effect of partially wetted surfaces on the total  $ET$ .

Previously, Lagos et al. [2,26] modified and extended the Ch-Mon model for partially vegetated surfaces to include the partition of  $ET$  into soil/residue evaporation and plant transpiration. However, in this approach,  $\lambda E_{soil}$  has not yet been separated into areas that are irrigated and areas that are not wetted by commonly used micro-irrigation systems. A previous attempt to include partially wetted soil areas in estimating total  $ET$  was made [27] using the dual crop coefficient and reference  $ET$  method, but to our knowledge, there are no other approaches with which a SEB model can separate  $\lambda E_{soil}$  from wetted and non-wetted ground floor areas.

This research proposes to build upon a multiple-layer surface energy balance model for estimating  $ET$  in partially wetted crop surfaces (SEB-PW), while accounting for the effects of soil evaporation on the total  $ET$ . This article describes the conceptual model development and the sensitivity analysis conducted on the model parameters and variables. The model performance was evaluated by comparing simulated values of  $ET$ ,  $\lambda E_{soil}$ , and  $T$  with field measurements conducted with surface renewal systems and micro-lysimeters in two micro-irrigated wine grape vineyards in Northern California. In addition, the model performance is compared to predictions of  $ET$  and  $\lambda E_{soil}$  from the S-W approach.

## 2. Materials and Methods

### 2.1. The Modified SEB-PW Model

Similar to previous multiple-layer model approaches [25,26], the modified SEB-PW model has four layers (Figure 1): The first layer extends from the reference height above the vegetation to the sink for momentum within the canopy; a second layer spans between the canopy and the soil surface, followed by a third layer comprising the top soil layer, where the surface resistance can be calculated as a function of the soil water content. Finally, the fourth layer includes a lower soil layer, where the soil atmosphere is nearly saturated with water vapor [2]. The SEB-PW model distributes net radiation ( $Rn$ ) into latent and sensible heat ( $\lambda E$  and  $H$ ), as well as soil heat ( $G$ ) fluxes through the soil–canopy system, according to the energy balance:

$$Rn - \lambda E - H - G = 0 \quad (1)$$

$$H = H_c + H_{bs} + H_s \quad (2)$$

$$\lambda E = \lambda E_c + \lambda E_{bs} + \lambda E_s \quad (3)$$

where  $H_c$ ,  $H_{bs}$ , and  $H_s$  are the sensible heat from the canopy, bare soil, and soil shaded below the canopy ( $W\ m^{-2}$ ), respectively, and  $\lambda E_c$ ,  $\lambda E_{bs}$ , and  $\lambda E_s$  are the latent heat from the canopy, the bare soil between rows, and the soil below the canopy soil ( $W\ m^{-2}$ ), respectively. Physical and chemical energy storage terms in the canopy–soil system are not considered [28]. Horizontal gradients of the potentials are assumed to be small enough for lateral fluxes to be ignored.

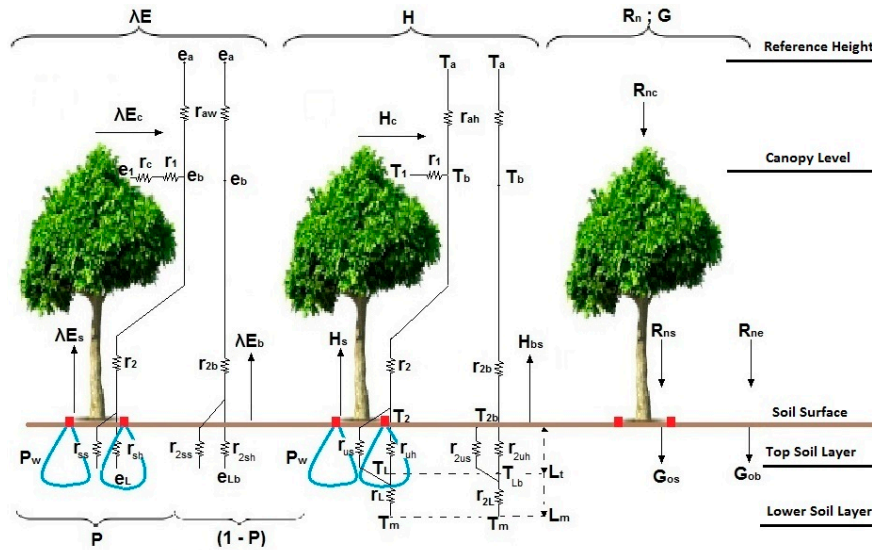


**Figure 1.** Schematic of fluxes and resistance network of the surface energy balance model for partially wetted soil (SEB-PW). Red dots and blue lines represent drippers and wetted soil zones, respectively.

Following Lagos et al. [2], the total net radiation, sensible, and latent heat flux are calculated, rather than adding a wet soil fraction ( $P_w$ ) in the SEB-PW model. Thus, the latent heat flux from the bare soil between the rows and soil under the canopy becomes:

$$\lambda E_s = \lambda E_{ss} \cdot (1 - P_w) + \lambda E_{sh} \cdot (P_w) \tag{4}$$

$$\lambda E_{bs} = \lambda E_{bss} \cdot (1 - P_w) + \lambda E_{bsh} \cdot (P_w) \tag{5}$$

where  $P_w$  is the wet soil fraction ( $0 < P_w < 1$ ),  $\lambda E_{ss}$  and  $\lambda E_{sh}$  are the soil evaporation under the canopy for non-wetted and wetted areas ( $W m^{-2}$  and  $W m^{-2}$ ), respectively, and  $\lambda E_{bss}$  and  $\lambda E_{bsh}$  are the soil evaporation for the bare soil between the rows under non-wetted and wetted conditions ( $W m^{-2}$  and  $W m^{-2}$ ), respectively (see Figure 2).

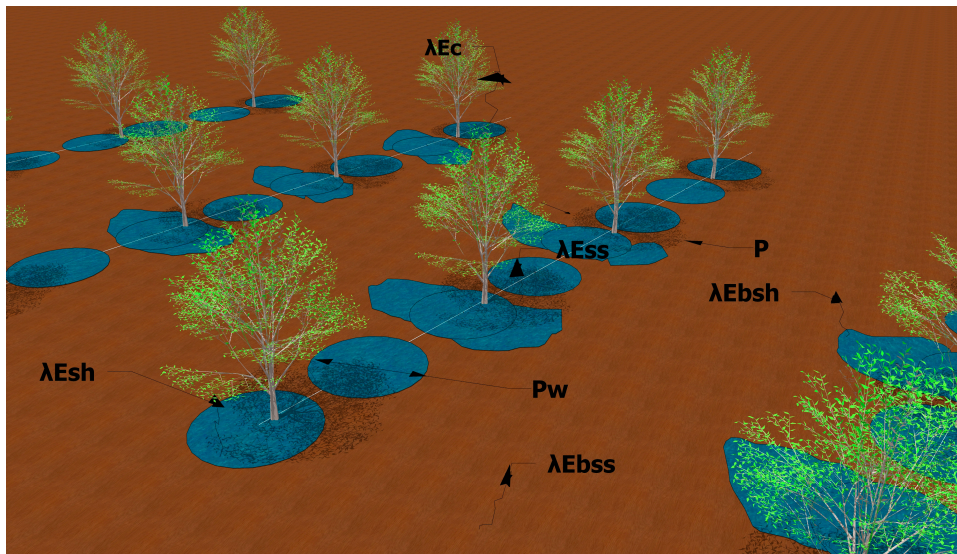


**Figure 2.** Schematic of soil evaporation from bare soil between rows and from non-wetted and wetted soil under the plant canopy.  $P$  is the fraction of the soil shadowed by plant canopy at solar noon ( $0 < P < 1$ ).

The differences in vapor pressure and temperature between levels can be expressed with an Ohm's law analogy using appropriate resistance and flux terms (Figure 1). The differences in saturation vapor pressure between points in the system have been calculated as linear functions of the corresponding temperature differences. A single value of the slope of the saturation vapor pressure ( $\Delta$ ), when evaluated in relation to the air temperature ( $T_a$ ), gave acceptable results for the components of the heat balance [2,25]. As such, vapor pressure can be obtained by:

$$\begin{aligned} e_1^* - e_b^* &= \Delta \cdot (T_1 - T_b) \\ e_L^* - e_b^* &= \Delta \cdot (T_L - T_b) \\ e_b^* - e_a^* &= \Delta \cdot (T_b - T_a) \\ e_{Lb}^* - e_b^* &= \Delta \cdot (T_{Lb} - T_b) \end{aligned} \quad (6)$$

where  $\Delta$  is the slope of the saturation vapor pressure with respect to the temperature curve between two points ( $\text{kPa } ^\circ\text{C}^{-1}$ );  $e_1^*$  is the saturation vapor pressure at the canopy ( $\text{kPa}$ );  $e_b^*$  is the saturation vapor pressure of the atmosphere at the canopy level ( $\text{kPa}$ );  $e_L^*$  is the saturation vapor pressure at the top of the under canopy irrigated layer ( $\text{kPa}$ );  $e_a^*$  is the saturation vapor pressure at the reference height ( $\text{kPa}$ );  $e_{Lb}^*$  is the saturation vapor pressure under the canopy at the top of the non-irrigated layer ( $\text{kPa}$ );  $T_1$  is the average temperature ( $^\circ\text{C}$ );  $T_b$  is the temperature within the canopy ( $^\circ\text{C}$ );  $T_L$  is the temperature at the interface between the upper and lower layer for the under canopy soil ( $^\circ\text{C}$ );  $T_a$  is the air temperature at the height of reference ( $^\circ\text{C}$ ); and  $T_{Lb}$  is the temperature at the interface between the upper and lower layer for the bare soil ( $^\circ\text{C}$ ).

The Equation (6) were combined and solved to estimate the energy fluxes. The solution gives the latent and sensible heat fluxes from the canopy as

$$\lambda E_c = \frac{R_{nc} \cdot \Delta \cdot r_1 + \rho \cdot C_p \cdot (e_b^* - e_b)}{\gamma \cdot (r_1 + r_c) + \Delta \cdot r_1} \quad (7)$$

$$H_c = \frac{R_{nc} \cdot \gamma \cdot (r_1 + r_c) - \rho \cdot C_p \cdot (e_b^* - e_b)}{\gamma \cdot (r_1 + r_c) + \Delta \cdot r_1} \quad (8)$$

where  $R_{nc}$  is the net radiation absorbed by the canopy ( $\text{W m}^{-2}$ );  $\rho$  is the density of moist air ( $1.013 \text{ kg m}^{-3}$ );  $C_p$  is the specific heat of air ( $1013 \text{ J kg}^{-1} \text{ } ^\circ\text{C}^{-1}$ );  $\gamma$  is the psychrometric constant ( $\text{kPa } ^\circ\text{C}^{-1}$ );  $e_b$  is the vapor pressure of the atmosphere at the canopy level ( $\text{kPa}$ );  $r_1$  is aerodynamic resistance between the canopy and the air ( $\text{s m}^{-1}$ ); and  $r_c$  is the surface canopy resistance ( $\text{s m}^{-1}$ ).

Similarly, latent and sensible heat fluxes under the canopy are estimated by:

$$\lambda E_s = \frac{R_{nDC} \cdot \Delta \cdot r_L \cdot r_2 + \rho \cdot C_p \cdot (e_b^* - e_b) \cdot (r_{us} + r_{uh} + r_L + r_2) - \rho \cdot C_p \cdot \Delta \cdot (T_b - T_m) \cdot (r_{us} + r_{uh} + r_2)}{\gamma \cdot r'_A \cdot (r_{us} + r_{uh} + r_L + r_2) + \Delta \cdot r_L \cdot (r_{us} + r_{uh} + r_2)} \quad (9)$$

$$H_s = \frac{R_{nDC} \cdot \Delta \cdot r_L - \lambda E_s \cdot (\Delta \cdot r_L + \gamma \cdot r'_A) + \rho \cdot C_p \cdot (e_b^* - e_b) - \rho \cdot C_p \cdot \Delta \cdot (T_b - T_m)}{\Delta \cdot r_L} \quad (10)$$

where  $R_{nDC}$  is the net radiation below the canopy ( $\text{W m}^{-2}$ );  $r_L$  is the soil heat flux resistance for the lower layer under the canopy area ( $\text{s m}^{-1}$ );  $r_2$  is the aerodynamic resistance between the canopy and the air at the canopy level ( $\text{s m}^{-1}$ );  $r_{us}$  and  $r_{uh}$  are the soil heat flux resistances under the canopy for the non-irrigated and irrigated upper layer ( $\text{s m}^{-1}$  and  $\text{s m}^{-1}$ ), respectively;  $T_m$  is the soil temperature at the bottom of the lower layer ( $^\circ\text{C}$ ); and  $r_{ss}$  and  $r_{sh}$  are the resistances to the diffusion of water vapor under the canopy at the non-wetted and wetted top soil layer ( $\text{s m}^{-1}$  and  $\text{s m}^{-1}$ ), respectively. The coefficient  $r'_A$  is defined in Appendix A.

Thus, the latent and sensible heat fluxes from the bare soil between rows are estimated by:

$$\lambda E_{bs} = \frac{R_{ne} \cdot \Delta \cdot r_{2L} \cdot r_{2b} + \rho \cdot C_P \cdot (e_b^* - e_b) \cdot (r_{2us} + r_{2uh} + r_{2L} + r_{2b}) - \rho \cdot C_P \cdot \Delta \cdot (T_b - T_m) \cdot (r_{2us} + r_{2uh} + r_{2b})}{\gamma \cdot r_B' \cdot (r_{2us} + r_{2uh} + r_{2L} + r_{2b}) + \Delta \cdot r_{2L} \cdot (r_{2us} + r_{2uh} + r_{2b})} \quad (11)$$

$$H_{bs} = \frac{R_{ne} \cdot \Delta \cdot r_{2L} - \lambda E_{bs} \cdot (\Delta \cdot r_{2L} + \gamma \cdot r_B') + \rho \cdot C_P \cdot (e_b^* - e_b) - \rho \cdot C_P \cdot \Delta \cdot (T_b - T_m)}{\Delta \cdot r_{2L}} \quad (12)$$

where  $R_{ne}$  is the net radiation absorbed by the soil between rows ( $W m^{-2}$ );  $r_{2L}$  is the soil heat flux resistance for the lower layer from the bare soil ( $s m^{-1}$ );  $r_{2b}$  is the aerodynamic resistance between the air around the bare soil and the canopy height and bare soil level ( $s m^{-1}$ );  $r_{2us}$  and  $r_{2uh}$  are the bare soil heat flux resistance for the non-wetted and wetted upper layer ( $s m^{-1}$  and  $s m^{-1}$ ), respectively; and  $r_{2ss}$  and  $r_{2sh}$  are the resistances to the diffusion of water vapor of bare soil at the non-wetted and wetted top soil layer ( $s m^{-1}$  and  $s m^{-1}$ ), respectively. The coefficient  $r_B'$  is defined in Appendix A.

To calculate the values of the latent and sensible heat flux, it is necessary to know  $T_b$  and  $e_b$ ; these parameters can be expressed as:

$$e_b = \left[ \frac{X'}{\rho \cdot C_P} + T_b \cdot (\Delta \cdot Y' - Z') - \Delta \cdot T_a \cdot Y' + e_a^* \cdot Y' + T_m \cdot Z' + \frac{e_a}{\gamma \cdot r_{aw}} \right] \cdot \left[ \frac{\gamma \cdot r_{aw}}{1 + Y' \cdot r_{aw} \cdot \gamma} \right] \quad (13)$$

$$T_b = \left( \frac{J'}{\rho \cdot C_P} + T_a \cdot \left( \Delta \cdot M' + \frac{1}{r_{ah}} \right) - e_a^* \cdot M' + e_b \cdot M' - T_m \cdot N' \right) \cdot \left( \frac{r_{ah}}{1 - r_{ah} \cdot N' + r_{ah} \cdot \Delta \cdot M'} \right) \quad (14)$$

where  $e_a$  is the vapor pressure at the reference height (kPa);  $r_{aw}$  is the aerodynamic resistance for the water vapor transport ( $s m^{-1}$ ); and  $r_{ah}$  is the aerodynamic resistance for the heat transport ( $s m^{-1}$ ). The coefficients,  $J'$ ,  $M'$ ,  $N'$ ,  $X'$ ,  $Y'$ , and  $Z'$  involved in these expressions depend on environmental conditions and other parameters (see Appendix A).

These relationships define the SEB-PW model, which is applicable to orchards and vineyards with partial ground cover by crop vegetation, considering partially wetted soil, which are conditions typically occurring in micro-irrigated orchard systems. Without the wet soil fraction, the model only describes the energy balance and flux resistances for the surfaces covered by the canopy and residues [2].

## 2.2. SEB-PW Model Parameters

### 2.2.1. Aerodynamic Resistances

The aerodynamic resistance for the heat transport ( $r_{ah}$ ) and water vapor transport ( $r_{aw}$ ) can be expressed as [29,30]:

$$\begin{aligned} r_{ah} &= r_{am} + r_{bh} \\ r_{aw} &= r_{am} + r_{bw} \end{aligned} \quad (15)$$

where  $r_{am}$  is the aerodynamic resistance to momentum transfer ( $s m^{-1}$ );  $r_{bh}$  is the excess resistance terms for heat ( $s m^{-1}$ ); and  $r_{bw}$  is the excess resistance term for the water vapor transfer ( $s m^{-1}$ ).

The theoretical relationship, proposed by Shuttleworth and Gurney [31], may be used to estimate the aerodynamic resistance  $r_{am}$  by integrating the eddy diffusion coefficient over the sink of momentum in the canopy ( $z_o + d'$ ) with a reference height above the canopy ( $z_o$ ):

$$r_{am} = \frac{1}{k \cdot u^*} \cdot \ln \left[ \frac{z_r + d'}{h - d'} \right] + \frac{h}{n \cdot K_h} \cdot \left[ \exp \left[ n \cdot \left( 1 - \frac{z_o + d'}{h} \right) \right] - 1 \right] \quad (16)$$

where  $k$  is the von Karman constant ( $k = 0.41$ );  $u^*$  is the friction velocity ( $m s^{-1}$ );  $z_r$  is the height above the canopy (m);  $d'$  is the zero plane displacement height (m);  $h$  is the height of vegetation (m);  $n$  is the attenuation coefficient (dimensionless);  $K_h$  is the value of the eddy diffusion coefficient at the top of

the canopy ( $\text{m}^2 \text{s}^{-1}$ ); and  $z_o$  is the surface roughness (m). The  $n$  value can be considered equal to 2.5 ( $n = 2.5$ ), which is a typical value recommended for agricultural crops [2,31].

The excess resistance for heat and water vapor transfer can be expressed as [32,33]:

$$r_{bh} = \frac{1}{k \cdot u^*} \cdot k \cdot B^{-1} \quad (17)$$

$$r_{bw} = \frac{k \cdot B^{-1}}{k \cdot u^*} \cdot \left[ \frac{k_1}{D_v} \right]^{\frac{2}{3}} \quad (18)$$

where  $B^{-1}$  is a dimensionless bulk parameter;  $k_1$  is the thermal diffusivity ( $\text{m}^2 \text{s}^{-1}$ ); and  $D_v$  is the molecular diffusivity of the water vapor in the air ( $\text{m}^2 \text{s}^{-1}$ ). Verma [32] considered that a first approximation for  $k \cdot B^{-1}$  is 2.0. Lhomme et al. [34] and Runkle et al. [35] recommended the use of values near to 2 when the leaf area index is equal to or bigger than 3. Additionally, Humphreys et al. [36] recommended the use of values near to 2 (1.6 and 2.3, the lower and higher values, respectively) in energy balance systems.

The aerodynamic resistance between the soil surface and the sink of the momentum below the canopy ( $r_2$ ) can be expressed as [31]:

$$r_2 = \frac{h \cdot \exp(n)}{n \cdot K_h} \cdot \left[ \exp\left(\frac{n \cdot z'_0}{h}\right) - \exp\left(\frac{-n \cdot (z_o + d')}{h}\right) \right] \quad (19)$$

where  $z'_0$  is the roughness length of the soil surface (m). The surface roughness ( $z_o$ ) and the zero-plane displacement height ( $d'$ ) are related to the leaf area index (LAI) as:

$$\begin{aligned} z_o &= z'_0 + 0.3 \cdot h \cdot X^{\frac{1}{2}}, & 0 \leq X \leq 0.2 \\ z_o &= 0.3 \cdot h \cdot \left(1 - \frac{d'}{h}\right), & 0.2 < X \leq 1.5 \\ d' &= 1.1 \cdot h \cdot \ln\left(1 + X^{\frac{1}{4}}\right), & X = C_d \cdot LAI \end{aligned} \quad (20)$$

where  $C_d$  is the average drag coefficient for the individual leaves.

Brenner and Incoll [37] reported that, when  $P$  is equal to zero, the aerodynamic resistance in the bare soil ( $r_{2b}$ ) will be assumed to be  $r_a^b$ , and when  $P$  is equal to 1,  $r_{2b}$  will be equal to  $r_2$ . Therefore, the relationship of  $r_{2b}$  varies linearly between  $r_2$  and  $r_a^b$  as:

$$\begin{aligned} r_{2b} &= P \cdot r_2 - (1 - P) \cdot r_a^b \\ r_a^b &= \frac{\ln\left(\frac{z_m}{z_o}\right)}{k^2 \cdot u} \end{aligned} \quad (21)$$

## 2.2.2. Canopy Resistances

The average boundary layer resistance of the canopy ( $r_1$ ) for the latent and sensible heat flux is influenced by the surface area of vegetation [17]:

$$r_1 = \frac{r_b \cdot \sigma_b}{LAI} \quad (22)$$

where  $r_b$  is the resistance of the leaf boundary layer ( $\text{s m}^{-1}$ ), which is proportional to the temperature difference between the leaf and surrounding air, divided by the associated flux [2]. Averaging the drag coefficient for the individual leaves,  $\sigma_b$  is a damping factor equal to 0.5 [38]. The resistance of the leaf boundary layer ( $r_b$ ) can be expressed as [38]:

$$r_b = \frac{100}{n} \left(\frac{w}{u_h}\right)^{\frac{1}{2}} \cdot \left[1 - \exp\left(\frac{-n}{2}\right)\right]^{-1} \quad (23)$$

where  $w$  is the representative leaf width (m) and  $u_h$  is the wind speed at the top of the canopy ( $\text{m s}^{-1}$ ). Shuttleworth and Wallace [17] indicated that  $r_b$  depends on the wind velocity inside the canopy, and the typical value is  $25 \text{ s m}^{-1}$ . Normally, when using  $r_b = 25 \text{ s m}^{-1}$  with  $LAI = 4$ , the corresponding canopy boundary layer resistance is  $r_1 = 3 \text{ s m}^{-1}$ .

Stannard [19] proposed a model to estimate the canopy surface resistance ( $r_c$ ) in the function of  $LAI$ , vapor pressure deficit ( $VPD$ ), and solar radiation ( $R_S$ ). However, a similar model, with an exponential relation between  $r_c$  and  $VPD$ , can be used to express the canopy resistance [39]:

$$r_c = \left[ \frac{C_1 \cdot LAI}{LAI_{max}} \cdot \frac{C_2}{1 - \exp(-VPD)} \cdot \frac{R_S \cdot (R_{Smax} + C_3)}{R_{Smax} \cdot (R_S + C_3)} \right]^{-1} \quad (24)$$

where  $C_1$ ,  $C_2$ , and  $C_3$  are regression coefficient constants;  $LAI_{max}$  is the maximum value of  $LAI$ ; and  $R_{Smax}$  is the maximum value of solar radiation (estimated at  $1000 \text{ W m}^{-2}$ ). It is worth emphasizing that this relationship does not account for the soil water stress effects [2].

### 2.2.3. Soil Resistances

In a surface soil layer of thickness  $L_t$ , the resistance to vapor flux from the diffused evaporating sites to the surface varies from very low, for saturated soil, to an upper limit for entirely dry soil [18]. Several studies in the past related the bare soil resistance ( $r_{ss}$ ,  $r_{2ss}$ ,  $r_{sh}$ , and  $r_{2sh}$ ) with the volumetric soil water content [40–42]. Previous studies have been conducted to investigate  $r_{ss}$ ,  $r_{2ss}$ ,  $r_{sh}$ , and  $r_{2sh}$  and commonly express them as a function of the soil water content, such as linear, exponential, or power functions. In this study, similar to Zhao et al. [21], the power function was determined as  $r_{ss}$ ,  $r_{2ss}$ ,  $r_{sh}$ , and  $r_{2sh}$  by:

$$r_i = a \cdot \left( \frac{\theta_{sat}}{\theta_i} \right)^b \quad (25)$$

where  $r_i$  is the soil surface resistance;  $\theta_i$  is the soil water content;  $\theta_{sat}$  is the saturated water content of the surface layer;  $a$  and  $b$  are the fitting parameters; and the sub-index  $i$  represent  $ss$ ,  $2ss$ ,  $sh$ , and  $2sh$  ( $ss$  and  $sh$  are the non-irrigated and irrigated soil below the canopy, respectively;  $2ss$  and  $2sh$  are the bare non-irrigated and irrigated soil, respectively).

According to Choudhury and Monteith [25], the bare soil and under-canopy soil resistances for the heat flux in the soil layer, extending from depth  $L_t$  to  $L_m$  ( $r_{2L}$  and  $r_L$ , respectively), can be estimated as

$$\begin{aligned} r_L &= \frac{\rho \cdot C_p \cdot (L_m - L_t)}{K_L} \\ r_{2L} &= \frac{\rho \cdot C_p \cdot (L_m - L_t)}{K_{2L}} \end{aligned} \quad (26)$$

where  $K_{2L}$  and  $K_L$  are the bare soil and under-canopy soil thermal conductivities in the soil layer, extending from depth  $L_t$  to  $L_m$  ( $\text{W m}^{-1} \text{ }^\circ\text{C}^{-1}$ ), respectively.

The bare soil and under-canopy soil resistance for the heat flux in the non-irrigated and irrigated soil layer, extending from the soil surface to  $L_t$  ( $r_{2us}$ ,  $r_{us}$ ,  $r_{2uh}$  and  $r_{uh}$ , respectively), can be obtained as:

$$r_j = \frac{\rho \cdot C_p \cdot L_t}{K'_j} \quad (27)$$

where  $r_j$  is the soil resistance for the heat flux;  $K'_j$  is the soil thermal conductivities in the soil layer, extending from the soil surface to  $L_t$ ; and the sub-index  $j$  represents  $us$ ,  $2us$ ,  $uh$ , and  $2uh$  ( $us$  and  $uh$  are the below-canopy non-irrigated and irrigated soil layer, respectively;  $2us$  and  $2sh$  are the non-irrigated and irrigated bare soil, respectively).

### 2.2.4. Net Radiation

The net radiation ( $R_n$ ), measured or estimated above the field, reflects the effect of the composite albedo of the canopy, soil under the canopy, and soil between the rows on incoming long and short wavelength solar radiation ( $R_{sL}$  and  $R_{sS}$ ). The SEB-PW model requires the partitioning of  $R_n$  into net radiation intercepted by the canopy surface ( $R_{nc}$ ), the net radiation below the canopy ( $R_{nDC}$ ) and the net radiation absorbed by the soil between the rows ( $R_{ne}$ ). Beer's law estimates the fraction of  $R_n$ , penetrating the canopy to the ground surface (under the canopy) as:

$$R_{nDC} = R_n \cdot \exp(-C_{ext} \cdot LAI) \quad (28)$$

where  $C_{ext}$  is the canopy extinction coefficient for  $R_n$  ( $C_{ext}$  value of 0.6 was used).

The  $R_{nc}$  is calculated as:

$$R_{nc} = R_n - R_{nDC} \quad (29)$$

This modified model estimates the effect and importance of dry and wet soil evaporation on the total ET and can better inform water balance studies to improve micro-irrigation management.

## 2.3. Model Evaluation

### 2.3.1. Study Sites

The SEB-PW model was applied to a pair of micro-irrigated study vineyards located in Northern California, where a team of researchers collected field measurements of  $ET$ ,  $E$ , and other bio-physical parameters over the course of the 2018 growing season. The two study sites are adjacent North (S1) and South-facing (S2) blocks of a commercial production vineyard (Figure 3) near Pilot Hill, El Dorado County, California ( $38^{\circ}48'7.2''$  N,  $121^{\circ}1'44.76''$  W; 381 m above sea level), approximately 72 km East of Sacramento in the foothills of the Sierra Nevada Mountains.



**Figure 3.** Aerial overview photo of the study vineyard blocks with North (S2) and South facing (S1) aspect, and locations of the evapotranspiration ( $ET$ ) measurement stations.

In both study blocks, the planting material was Cabernet sauvignon (clone 15) grafted onto *Vitis riparia* x *Vitis rupestris* cv. 3309 Couderc rootstock. The vines were trained in a bilateral cordon vertical shoot positioned system (VSP), and pruned to 14, 2-bud spurs per vine. The climate of El Dorado County is semi-arid. Both vineyard blocks lie on very rocky loam soil of the Auburn series [43], as mapped by the USDA-National Cooperative Soil Survey (SSURGO) [44]. Both sites are equipped

with a micro-irrigation system, consisting of single driplines with two pressure-compensating online button drippers (Netafim USA, Fresno, CA, USA) per vine with a nominal flowrate of  $1.9 \text{ L h}^{-1}$ . Other specific vineyard characteristics, for S1 and S2, are presented in Table 1.

**Table 1.** Micro-irrigated vineyards information and soil water properties for S1 and S2. Average soil water content at the permanent wilting point ( $\theta_{PMP_{avg}}$ ), field capacity ( $\theta_{FC_{avg}}$ ), average bulk density ( $\rho_{avg}$ ), average emitter's flowrate ( $Q_{avg}$ ), and distribution uniformity ( $DU$ ).

Variable	S1	S2
Plantation year		2000
Density of vines (vines $\text{ha}^{-1}$ )		3703
Spacing (m $\times$ m)		$1.8 \times 1.5$
Height of the canopy (m)	1.5	2.0
Size block (ha)	0.6	1.0
Depth of soil (m)		0.6
$\theta_{PMP_{avg}}$ ( $\text{m}^3 \cdot \text{m}^{-3}$ ) <sup>1</sup>	0.213	0.196
$\theta_{FC_{avg}}$ ( $\text{m}^3 \cdot \text{m}^{-3}$ ) <sup>1</sup>	0.350	0.346
$\rho_{avg}$ ( $\text{kg} \cdot \text{m}^{-3}$ ) <sup>1</sup>	1.40	1.38
Topographic slope (%)	25.4	24.5
System application rate ( $\text{mm h}^{-1}$ )	1.65	1.73
$Q_{avg}$ ( $\text{L h}^{-1}$ )	2.3	2.4
$DU$	0.87	0.86

<sup>1</sup> "Soil Water Characteristic" program USDA, WA.

The irrigation performance parameters from Table 1 were determined in April 2016 by a professional irrigation system evaluation team (Mobile Lab from the Natural Resource Conservation Service-Resource Conservation District) that used the micro-irrigation evaluation procedure developed by the Irrigation Training and Research Center (ITRC) of CalPoly [45]. In both vineyards (S1 and S2), the soil water tension (SWT) was measured continuously at two depths (0.3 and 0.6 m), with solid-state electrical resistance sensors (Watermark, Irrometer Company Inc., Riverside, CA, USA).

The midday stem water potential ( $\Psi_{SWP}$ ) was measured with weekly or bi-weekly frequency during the course of the 2018 growing season, using a Scholander-type pressure chamber (Model 615, PMS Instrument Co., Corvallis, OR, USA) on six vines randomly selected within the footprint area of each ET station. For each vine, a fully expanded and shaded leaf was selected and covered with light and moisture-impervious Mylar bags at least 20 min before performing the measurement to equilibrate with branch xylem water potential [46]. The  $\Psi_{SWP}$  measurements were conducted during clear-sky days between 11:00 am and 2:00 pm, by recording the pressure exerted in the chamber when the initial xylem sap was observed emerging from the cut-end petiole.

During the same dates of the  $\Psi_{SWP}$  measurements, the fraction of the shaded soil ( $P$ ), or light interception by the vine canopy, was measured using the Paso Panel canopy shade meter [47,48]. The Paso panel consists of a solar collector panel, a voltage meter, and power switch attached to a portable frame that can be held underneath the grapevine foliage for a few seconds to measure the light being intercepted by the vines canopy. The device measures the amount of current produced by the solar panel, which is proportional to the amount of sunlight striking its surface. On each date, the first measurements were taken outside the vineyard in full sun to record a baseline reading of incoming solar radiation. The panel was then placed under the vines canopy at multiple locations and the readings were then divided by the baseline radiation to determine the shaded area by the vine canopy, which is a proxy of the fractional canopy cover or fraction of shaded soil. All the measurements in the S1 and S2 vineyard blocks were taken during clear sky days at solar noon  $\pm 1$  h.

The wet soil fraction ( $P_w$ ) was measured on the soil surface each day, in the morning during the first and second field campaign, with a measuring tape. The leaf area index (LAI) was estimated using the method proposed by Williams and Ayars [47] from the fraction of the shadowed soil and crop coefficient.

### 2.3.2. Micrometeorological and Surface Renewal Measurements

Two *ET* stations were installed (one station per site, Figure 3) to measure and record the surface energy balance (SEB) components and micro-meteorological variables at 30 min intervals using a data logger (CR1000, Campbell Scientific Inc., Logan, UT, USA). The  $\lambda E$  was determined with the residual of SEB method that calculates  $\lambda E$  as the residual from  $R_n$ ,  $G$ , and  $H$  measured at the study sites with micro-meteorological sensors.

Each *ET* station included: A net radiometer (NRLite2, Kipp and Zonen Inc., Delft, the Netherlands) to measure  $R_n$ , a three-dimensional sonic anemometer (81,000, R.M. Young Inc., Traverse City, MI, USA) to measure  $H$  with the Eddy Covariance (EC) methodology (both approximately 1 m above the vine canopy), and two 76.2  $\mu\text{m}$  diameter Chromel-Constantan thermocouples (model FW3, Campbell Scientific Inc., Logan, UT, USA), both mounted approximately 2.35 m above the soil surface, to calculate  $H$  by the SR method,  $T_a$  was measured at 10 Hz frequency; three soil sensor packages to calculate  $G$ , each consisting of one soil heat flux plate (HFT3, REBS, Bellevue, Washington, USA), four averaging soil temperature thermocouple probes (TCAV, Campbell Scientific Inc., Logan, UT, USA), and one volumetric soil moisture sensor (EC5, Decagon Devices, Pullman, WA, USA). For each package, the ground heat flux plate and soil moisture sensor were installed horizontally at 0.05 m below the soil surface, whereas the probes of the TCAV sensor were installed at an angle from 0.04 to 0.01 m depth and were distributed on both sides of the HFT3 and EC5 sensors in a line perpendicular to the tree rows.

$\lambda E$  was calculated using  $H$  from the sonic anemometer, i.e.,  $H$  by Eddy Covariance and when no values were recorded with sonic anemometer,  $H$  was estimated from the thermocouple using the SR technique. About 91% of  $H$  values were obtained from the EC method. Due to the limited size of both vineyard blocks (Figure 3) and to assure that measured fluxes were mainly coming from the surface of interest, we evaluated the footprint at both sites. The footprint was calculated using the model proposed by Kljun et al. [49]. These analyses showed that 80% and 90% of the fluxes are mainly coming from the interest blocks for the EC method and SR technique, respectively. It is recognized that EC measurements are expected to be the most accurate over flat terrain where there is an extended homogenous surface upwind from the tower, but S1 and S2 are blocks facing Southwest and Northwest with slopes of 25.4 and 24.5%, respectively. Zitouna-Chebbi et al. [50] and Hiller et al. [51] evaluated the consistency of EC measurements collected in sloping conditions. Their results showed that, for their measurements, and especially for the upward flows, the energy balance closure was similar to that reported in the literature. For this evaluation and following Zitouna-Chebbi et al. [50] and Hiller et al. [51], we assumed that it is possible to yield realistic energy flux measurements under these conditions. The calibration procedure between SR and sonic anemometer analysis used in this research for computing  $H$  is described in detail by Shapland et al. [52] and Marino et al. [53]. A calibration factor ( $\alpha$ ) of 0.96 and 1.06 was found for S1 and S2 sites, respectively. Similar  $\alpha$  values were found by others studies over vineyards [52,54,55]. These results agree with Haymann et al. [56] where, for a cotton field, the SR technique was reliable in estimating sensible and latent heat fluxes and the weighting factor ( $\alpha$ ) was essentially independent of the geometrical fetch and the flux footprint of the sensors.

At each *ET* station, all the above-ground individual sensors were installed on a mounting frame consisting of steel posts, driven approximately 1 m into the ground, and steel cross arms. The height of the steel mounting frame was approximately 3.5 m from the vineyard floor. Direct two-way communication with the station was enabled through a cellular phone modem (RavenXT, Sierra Wireless, Richmond, BC, Canada).

### 2.3.3. Soil Evaporation

$\lambda E_{soil}$  is commonly measured with micro-lysimeters (ML) that are constructed with stainless steel or PVC pipes. Evett et al. [9] studied the effects of materials on evaporation, using cylindrical steel and plastic ML of 10, 20 and 30 cm lengths, and found that steel conducted heat more easily, and its surfaces were significantly cooler during the day and warmer at night than either plastic ML or the adjacent field soil. Therefore, ML walls should be made of nonconductive material, such as plastic, and

one should avoid changing its position when determining the spatial variability of evaporation over time. Todd et al. [10] also searched for the difference between plastic and steel MLs and found that the wall material affected temperature distribution but not evaporation. Similarly, Boast and Robertson [8] evaluated different lengths (44, 70, 106, and 146 mm) of MLs and found that 70 mm long MLs are accurate to within 0.5 mm for 1 or 2 days, depending on the initial soil wetness. Therefore, for this study, the soil evaporation was measured using MLs made of stainless-steel rings.

The MLs were 0.1 m high, with a diameter of approximately 0.076 m (cross-sectional area of 45.4 cm<sup>2</sup>). Each ML had a layer of insulation of PVC to prevent or minimize the lateral heat flux between the soil inside and outside the stainless-steel ring lysimeter [3,57]. The surface of each ML was leveled with the outside soil surface to minimize unnatural air flow in the near-ground boundary layer [58]. In S1 and S2, 12 MLs per site were installed, six between rows and six below the vines canopy. MLs were installed approximately 24 h after micro-irrigation events, and the undisturbed soil core was collected using stainless-steel rings. The samples were capped at the bottom, before being placed in a PVC sleeve and weighed every day between 08:00 and 10:00 a.m. using an electronic scale (Radwag WTC 2000, Data Support Company, Panorama city, CA, USA), with a precision of 0.01 g. The reason for collecting the undisturbed soil core after irrigation events and not before was to: (a) Allow the lateral redistribution of water to occur, especially under dry soil; (b) allow the soil to drain to a near-field capacity; and (c) eliminate the potential for suturing the MLs [57]. The measurements were performed over five days in two field campaigns, the first around mid-June (June 15–20, 2018), and the second across late June and early July (June 29–July 4, 2018). The soil evaporation from MLs was determined according to Feng et al. [59].

### 3. Results and Discussion

#### 3.1. Sensitivity Analysis

A sensitivity analysis of the predicted *ET* rates with the modified SEB-PW model was performed in relation to the parameter value changes. The effect of the changes in the parameters and model resistances were expressed as changes in *ET* (*LE*), changes in the crop transpiration ratio ( $T_{ratio}$ ), calculated as the ratio between  $\lambda E_c$  over *ET* ( $T_{ratio} = \lambda E_c / LE$ ), and changes in the evaporation ratio ( $E_{ratio}$ ), calculated as the ratio between the total soil evaporation ( $\lambda E_{soil}$ ) over the total *ET* ( $E_{ratio} = \lambda E_{soil} / ET$ ). The analyses were conducted based on typical half-day conditions during the growing season of a vineyard in Northern California (Table A1, see Appendix A). The sensitivity analysis of the SEB-PW model was performed for all model parameters, and the most relevant results are shown in Figures 4 and 5.

##### 3.1.1. Soil Resistances to Vapor Flux

Three values of  $r_{ss}$  and  $r_{sh}$  were used during the analysis, based on the scientific literature documenting that  $r_{ss}$  and  $r_{sh}$  have average values around 1000 and 200 s m<sup>-1</sup>, respectively [42,60]. To evaluate their effects on *ET*,  $\lambda E_{soil}$ ,  $T_{ratio}$ , and  $E_{ratio}$ ,  $r_{ss}$  and  $r_{sh}$  were changed by  $\pm 30\%$ . The effect of  $r_{ss}$  and  $r_{sh}$  on the total *ET* and  $T_{ratio}$  showed small differences (1%) under different *LAI* conditions. However, the resistances  $r_{ss}$  (Figure 4a) and  $r_{sh}$  (Figure 4b) had a higher effect on the total  $\lambda E_{soil}$  (3–22%). Comparing  $r_{sh}$  with  $r_{ss}$ , the resistance  $r_{sh}$  produced a more important change in  $\lambda E_{soil}$ , with differences between 11%–22% when  $r_{sh}$  varied by  $\pm 30\%$  (Figure 4b). These differences can be seen in Figure 4c,d. While  $r_{ss}$  showed no effect in  $T_{ratio}$  and  $E_{ratio}$  (Figure 4c),  $r_{sh}$  showed changes for all evaluated *LAI* conditions (Figure 4d). This is remarkably more important for *LAI* values lower than 0.1, where the  $E_{ratio}$  fraction is higher than  $T_{ratio}$  (Figure 4c,d).

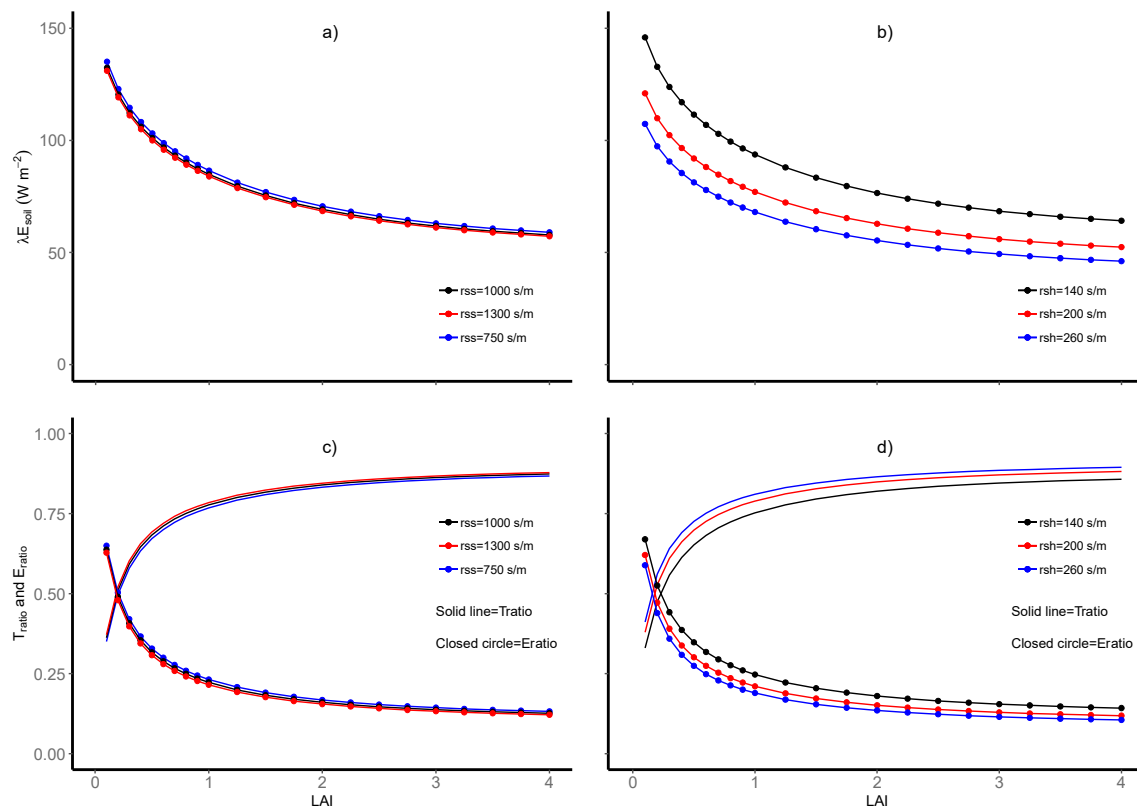


**Figure 4.** Soil latent heat flux ( $\lambda E_{soil}$ ) (a,b), crop transpiration ratio ( $T_{ratio}$ ), and soil evaporation ratio ( $E_{ratio}$ ) (c,d), estimated as a function of  $LAI$  for soil resistances to vapor flux under dry ( $r_{ss}$ ) and irrigated ( $r_{sh}$ ) conditions below the canopy.  $P = 0.5$  and  $P_w = 0.3$ .

### 3.1.2. Vapor Pressure Deficit, Canopy Resistance and Air Temperature

Three typical values of  $VPD$  in vineyards of Northern California were used to evaluate the effect on the total  $ET$ ,  $T_{ratio}$  and  $E_{ratio}$ . The values of  $VPD$  used were 1.23, 1.75, and 2.27 kPa under different  $LAI$  conditions. The results showed that the total  $ET$  was higher for  $VPD = 2.2$  kPa, with differences of 5% when  $LAI = 4.0$  (Figure 5a).  $T_{ratio}$  variations for  $VPD = 1.2$ , 1.75 and 2.2 kPa were between 1%–4%, with small differences for values of  $LAI < 0.1$  (Figure 5d).

The  $r_c$  is affected by changes in  $LAI$ ,  $VPD$ , and solar radiation (Equation (24)), and according with the literature,  $r_c$  frequently has values close to  $45 \text{ s m}^{-1}$  in well-irrigated vineyards [20,61]. Changes of  $\pm 40\%$  in  $r_c$  were used to evaluate the effect on the total  $ET$  under different  $LAI$  conditions. It was observed (Figure 5b) that the total  $ET$  was lower for higher  $r_c$  values. As expected, the  $r_c$  effect on the total  $ET$  for low  $LAI$  conditions ( $< 0.5$ ) was small (1%). However, more differences (10%–16%) were found when  $LAI > 2.0$  (Figure 5b). The effect of  $r_c$  on  $T_{ratio}$  showed a greater impact when  $LAI$  was between 1.0–4.0 (Figure 5e).

Similar to  $r_c$ ,  $T_a$  varied by  $\pm 5^\circ \text{C}$  in evaluating the effect on the total  $ET$  (Figure 5c). The results showed that high total  $ET$  occurs when  $T_a = 35^\circ \text{C}$ , compared to when  $T_a = 25^\circ \text{C}$ . Further, the effect on the total  $ET$  showed differences between 3%–11% when  $T_a$  varied by  $\pm 5^\circ \text{C}$  (Figure 5c). The differences of  $T_a$  on  $T_{ratio}$  and  $E_{ratio}$  were higher for values of  $LAI > 1.0$ , while fewer differences (2%–4%) were observed for  $LAI$  values  $< 1.0$  (Figure 5f).

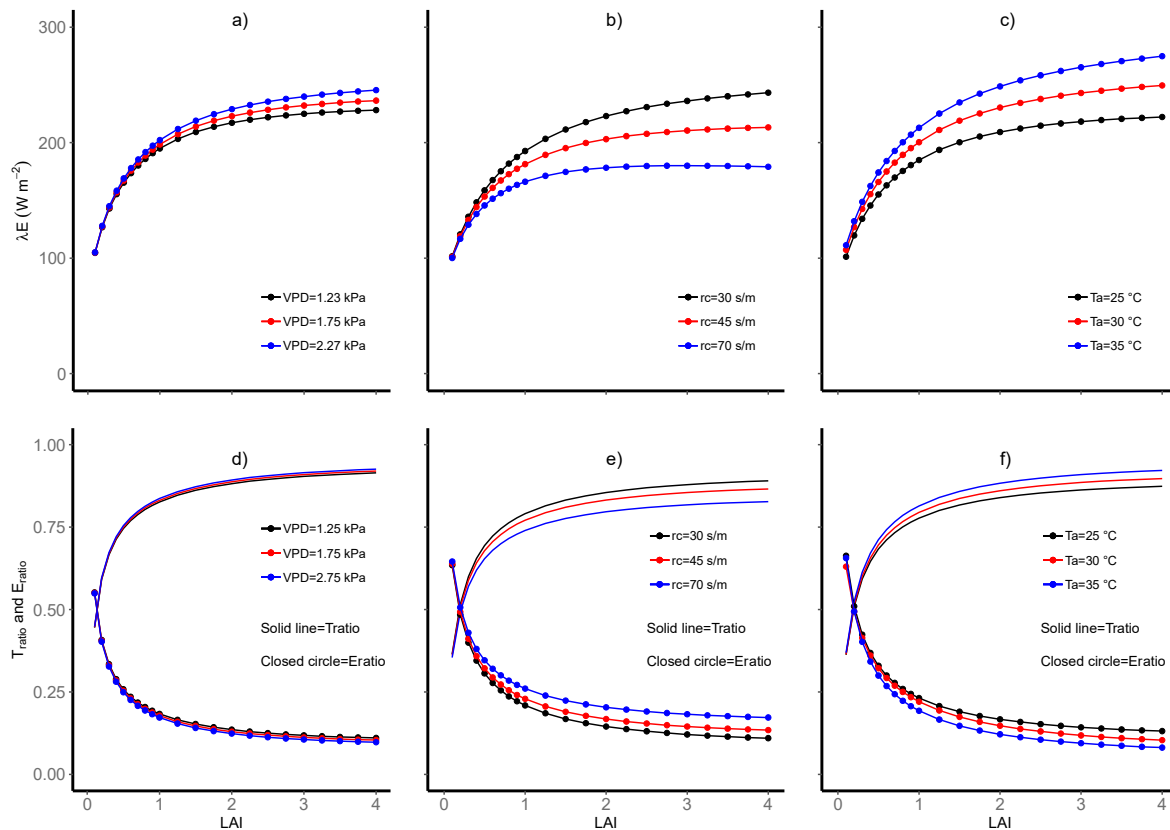


**Figure 5.** Latent heat flux ( $\lambda E$ ) (a–c), crop transpiration ratio ( $T_{ratio}$ ), and soil evaporation ratio ( $E_{ratio}$ ) (d–f), estimated as a function of LAI for vapor pressure deficit (VPD), canopy resistance ( $r_c$ ), and air temperature ( $T_a$ ).  $P = 0.5$  and  $P_w = 0.3$ .

In contrast to the previously analyzed parameters, the SEB-PW model was less sensitive to the soil heat flux resistances ( $r_{us}$  and  $r_{uh}$ ), the  $C_{ext}$  coefficient,  $T_m$ ,  $\alpha$ ,  $h$ , and  $r_L$  under different LAI conditions. The analysis showed that a  $\pm 30\%$  change of  $r_{us}$  and  $r_{uh}$  implied a minimum effect on the total ET (less than 1%). Similarly, three  $C_{ext}$  values (0.4, 0.6 and 0.8) were evaluated, and the results also showed a low sensitivity (0.5%–1.5%) to the total ET. These results agreed with the previous sensitivity analysis with similar parameters [2,20].

Canopy resistance represents a plant parameter that is affected by plant characteristics, e.g., LAI, plant height, and maturity. Soil factors and environmental factors also affect the canopy resistance [62]. Similarly,  $r_{ss}$  and  $r_{sh}$  are primarily affected by the soil texture and soil water content. As such, if the SEB-PW model is applied to a defined crop these important parameters need to be site-specifically calibrated, as indicated by the sensitivity analysis.

### 3.2. Preliminary Model Evaluation

Evapotranspiration simulated with the SEB-PW model was compared with measurements of ET using the surface renewal method (SR) [52]. The model evaluation is a two-step process that includes model calibration and model validation. As a result of the sensitivity analysis, parameters affecting the canopy resistance were calibrated to adjust to the modeled ET to SR measurements. For calibration purposes,  $r^2$ , RMSE, and  $d_a$  were evaluated. Specifically, observations from seven days before the first (7–14 June 2018) and second field campaigns (June 21 to 28, 2018) were considered to calibrate  $C_1$ ,  $C_2$ , and  $C_3$  coefficients in Equation (24). For soil evaporation, the  $a$  and  $b$  fitting parameter values in Equation (25) were selected from the scientific literature [21]. During calibration, the agreement between the measured and modeled ET was appraised by  $r^2$ , RMSE, and  $d_a$ , which were 0.94, 51  $W m^{-2}$ ,

and 0.96, respectively. Once the SEB-PW model was calibrated, the model was then evaluated using the soil evaporation measurements collected with MLs during the two five-day field campaigns.

### 3.2.1. Evapotranspiration and Soil Evaporation Measurement Field Campaign

#### Environmental, $SWT$ and $\Psi_{SWP}$ Conditions at the S1 and S2 Sites

The hourly data collected during the two five-day periods, with different  $P$  and  $P_w$  conditions ( $0.3 < P < 0.45$ ;  $0.1 < P_w < 0.5$ ), were used to compare the measured  $ET$  and  $E$  with the values predicted by the model at both sites (S1 and S2). The SEB-PW model requires hourly values for the net radiation ( $R_n$ ), wind speed ( $u$ ), air temperature ( $T_a$ ), relative humidity ( $RH$ ), soil temperature ( $T_s$ ), soil water content ( $\theta$ ), and solar radiation ( $R_s$ ).

During the first five-day measurement period (June 15–20, 2018), at the S1 site, the average air temperature was  $20.7 \pm 9.3$  °C, and the average wind speed was  $1.9 \pm 0.1$  m s<sup>-1</sup> (top S1, Table 2). At S2, the average air temperature was  $20.3 \pm 8.8$  °C, and the average wind speed was  $1.2 \pm 0.1$  m s<sup>-1</sup> (top S2, Table 2). During the second five-day measurement period (June 29–July 4, 2018), at both sites, the air temperature was similar to that of the first campaign, but the wind speed was slightly lower than the first campaign (Lower part of Table 2). Details of the hourly data are provided in Figure A1 of Appendix A.

The soil water tension ( $SWT$ ) at 0.3 m deep during the first field campaign at the S1 and S2 sites ranged between 20 and 110 cbar and 2 and 70 cbar, respectively. Similarly, for the second campaign, at S1 and S2, the  $SWT$  ranged from 17 to 61 cbar and 2 to 30 cbar, respectively (Table 2). In general, the S2 site had a higher soil water content than that of S1.

**Table 2.** Average air temperature ( $T_{a\ avg}$ ), average wind speed ( $u_{avg}$ ), and soil water tension ( $SWT$ ) data at the S1 and S2 sites during the first and second field campaigns.

Date (m/d/y)	S1			S2		
	$T_{a\ avg}$ (°C)	$u_{avg}$ (m s <sup>-1</sup> )	$SWT$ (cbar)	$T_{a\ avg}$ (°C)	$u_{avg}$ (m s <sup>-1</sup> )	$SWT$ (cbar)
6/15/2018	21.8	2.2	58	21.1	1.1	25
6/16/2018	19.1	2.5	70	19.0	1.2	36
6/17/2018	15.7	1.8	82	15.7	1.1	45
6/18/2018	20.3	1.7	95	19.3	1.7	54
6/19/2018	23.3	1.6	107	22.8	1.0	62
6/20/2018	24.0	1.9	110	23.7	1.1	70
	S1			S2		
6/29/2018	23.8	1.3	17	23.2	1.8	2
6/30/2018	27.0	1.8	27	26.2	2.0	10
7/1/2018	27.5	1.7	35	26.9	1.2	15
7/2/2018	24.3	1.8	44	24.0	1.1	19
7/3/2018	21.6	2.0	52	21.6	1.1	23
7/4/2018	18.6	1.7	61	18.3	1.0	27

Midday  $\Psi_{SWP}$  was measured at both sites once per week during June and July 2018. During the first field campaign, the  $\Psi_{SWP}$  values one day after irrigation were  $-0.62$  and  $-0.48$  MPa at S1 and S2, respectively, and five days after irrigation,  $\Psi_{SWP}$  values were  $-0.58$  and  $-0.47$  MPa for S1 and S2, respectively. During the second field campaign, the  $\Psi_{SWP}$  values were slightly lower values than those measured during the first field campaign.  $\Psi_{SWP}$  value higher than  $-0.7$  bar is normally considered as a non-stress condition for a Cabernet sauvignon vineyard [63].

#### Surface Energy Balance Measurements

Figure 6 shows the hourly values of the surface energy balance parameters during both field campaigns. Both the first and the second field campaigns were conducted after an irrigation event at

both sites. During the first field campaign, the  $T_a$  and  $VPD$  were lower (15% and 30%, respectively) than those during the second campaign. While during the first campaign, the daily averages of the fraction  $H/R_n$  were 40% and 36% at S1 (Figure 6a) and S2 (Figure 6b), respectively, during the second campaign, the average  $H/R_n$  fraction was 33% and 18% at S1 (Figure 6c) and S2 (Figure 6d), respectively. Since the greatest portion of the net radiation is converted into latent heat flux,  $H$  is often small in well-irrigated crop systems. At both sites,  $H/R_n$  was frequently lower during the first and second day after irrigation, while  $LE$  was higher, compared to the fourth day after irrigation. This result is consistent with the analysis of a well-watered crop, where, during three complete growing seasons, the ratio of  $H/R_n$  ranged from 15%–20% [64].

The average daily  $R_n$  is the mean amount of solar and terrestrial energy impinging upon the surface minus the energy reflected or emitted away from the surface over the course of a day. During the summer in California, the mean daily  $R_n$  is positive over all vegetation [52]. The average daily  $R_n$  was slightly higher at the S1 site (Figure 6a,c), compared with that at S2 (Figure 6b,d).

The average daily  $G$  during the summer in California is positive [52]. The S2 site (Figure 6b) had the lowest average daily  $G$  of  $1.3 \text{ W m}^{-2}$ , compared with S1 (Figure 6a), where the average daily  $G$  was  $7.2 \text{ W m}^{-2}$  during the first field campaign. Similar values were measured during the second campaign. The  $R_n$  was slightly lower at S2, so there was less energy available to contribute to  $G$  than at S1. In general,  $G$  was the smaller energy component of the surface energy balance, and less significant in terms of  $LE$  variability. Daily summations of  $G$  mostly hovered around zero for both field campaigns, as expected according to scientific literature [65,66].

The average daily  $LE$  is the mean amount of energy used to vaporize water from crops and soil surface over the course of a day. Over partially covered orchards and vineyards, which mostly consist of bare dry ground, more water is vaporized than condensed, so  $LE$  is positive [52]. S2 shows a slightly higher  $LE$  with respect to S1, for both field campaigns, which is in agreement with the higher  $SWT$  measured at S1 (Table 2). Similar results were found in a vineyard by Parry et al. [66] and Shapland et al. [52] at sites with the same row orientation.

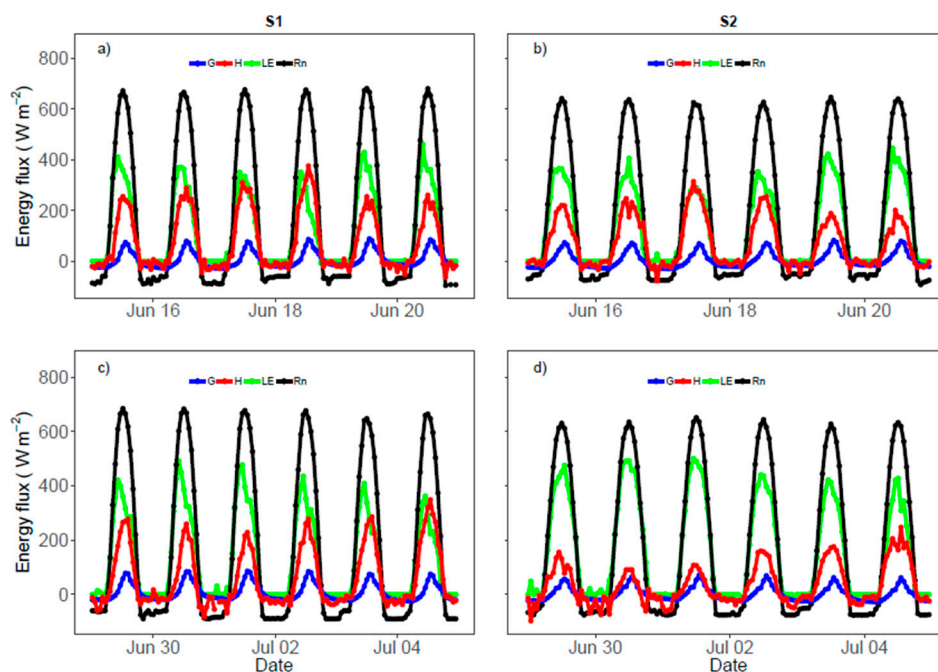


**Figure 6.** Diurnal trend of energy flux during a 12-day period (first field campaign (a,b): June 15–20 and second field campaign (c,d): June 29–July 4) at S1 and S2. Net radiation ( $R_n$ ), sensible ( $H$ ), latent ( $LE$ ), and soil heat flux ( $G$ ).

## Model Performance

$LE$  and  $\lambda E_{soil}$ , estimated with the SEB-PW model and  $LE$  measured using the SR method during the first field campaign are shown in Figure 7a,b. At midday, the maximum  $LE$  fluxes at S1 (Figure 7a) and S2 (Figure 7b) recorded during 20 June were 460 and 450  $W m^{-2}$ , respectively. In contrast, lower  $LE$  rates were found at midday on 17 June, with 350 and 290  $W m^{-2}$ , respectively. Similar hourly dynamics have been found in vineyards for days with similar environmental conditions [20,52,60]. At both sites (S1 and S2), the diurnal dynamics of the  $LE$ , estimated with the SEB-PW model, and  $LE$ , measured with the SR system, are similar. At both sites, higher differences of  $LE$ , estimated with the model, and  $LE$  measurements were found for days with higher  $T_a$  (24–28 °C) and higher  $VPD$  (2.5–4.0 kPa). In general,  $ET$  estimated with the SEB-PW were slightly smaller than the values measured at both sites. Poblete–Echeverría and Ortega–Fariás [60] also found that the clumped model tended to underestimate  $LE$  under clear sky conditions and with  $VPD$  of 2.1 and 3.1 kPa, respectively. As expected,  $\lambda E_{soil}$  was higher on the first day after irrigation and decreased during the next days. The weighted average of soil evaporation immediately after the irrigation event was 28% and 46% of the total  $ET$  at S1 and S2, respectively.

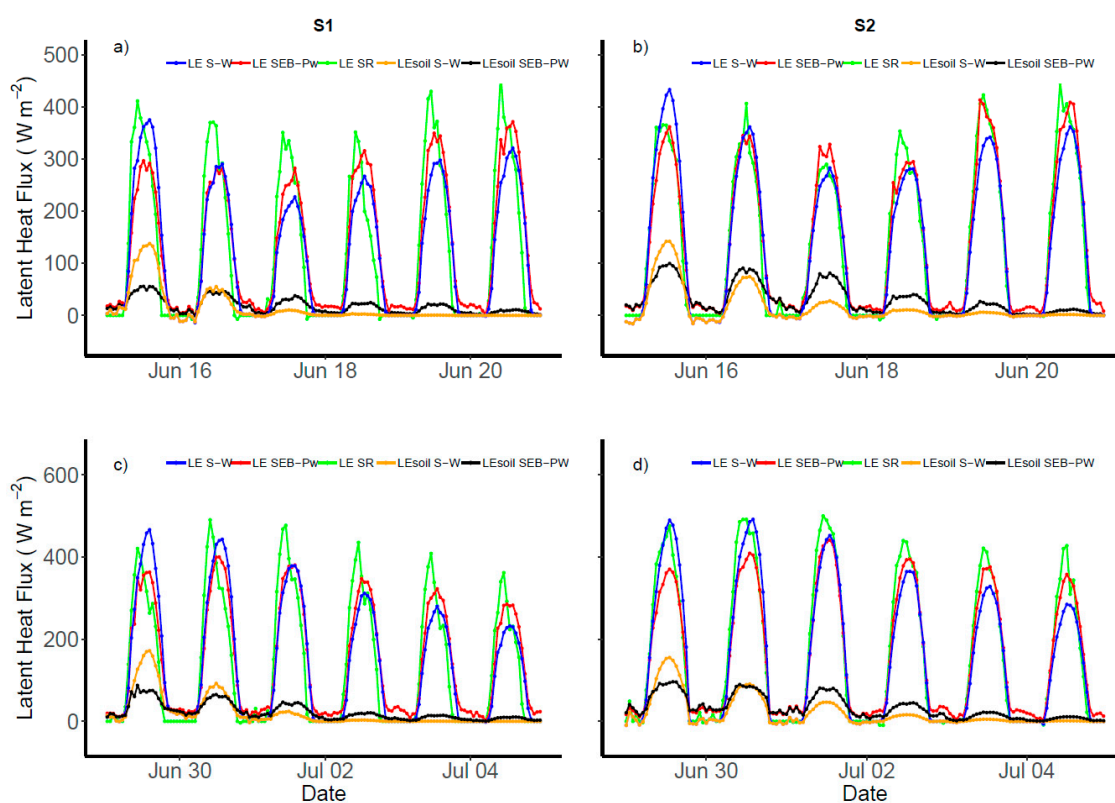


**Figure 7.** Values of evapotranspiration and soil evaporation estimated by the SEB-PW ( $LE_{SEB-PW}$  and  $LE_{soil SEB-PW}$ ) and the S-W ( $LE_{S-W}$  and  $LE_{soil S-W}$ ) models and evapotranspiration measured by the SR system ( $LE_{SR}$ ) during the first (a,b) and second (c,d) field campaigns.

During the second field campaign,  $LE$  and  $\lambda E_{soil}$  estimated by the SEB-PW model, and  $LE$  measured using the SR method, are shown in Figure 7c,d. Compared to the first campaign, the rates of  $LE$  estimated with the SEB-PW model were similar to the values measured with the SR station. The estimated  $LE$  were noticeably smaller than the measured values for S2 during the first three days, with higher values of  $T_a$  and  $VPD$  (Figure 7d). Similarly,  $\lambda E_{soil}$  was higher the first day after irrigation and decreased during the next days. The weighted average of soil evaporation immediately after the irrigation event was 35% and 45% of the total  $ET$  at S1 and S2, respectively.

Similarly, during both field campaigns, the S-W model was used to estimate  $LE$  and  $\lambda E_{soil}$  (Figure 7). The S-W model was selected because it has been successfully applied to estimate  $ET$  in vineyards by several previous studies [20,21,23]. Results showed that, in general, the S-W model also tended to underestimate  $LE$ . When compared to the SEB-PW model, the S-W approach was higher on the first two days after the irrigation event, and in the following days, the S-W model estimated lower values of  $LE$  than those predicted by SEB-PW. As expected, and similar to SEB-PW, the  $\lambda E_{soil}$  was higher on the first day after irrigation and decreased during the next days.

The hourly measurements and SEB-PW predictions for both campaigns at both sites were analyzed to evaluate the model's performance (Figure 8). The index  $d_a$ ,  $RMSE$ ,  $r^2$ ,  $MAE$ , and  $C_{NS}$  were used for model evaluation [67,68]. The first field campaign showed a coefficient of determination of 0.88 and 0.97 for S1 (Figure 8a) and S2 (Figure 8b), with a slope of regression of 0.86 and 0.98, respectively. The second field campaign showed an  $r^2$  of 0.89 for S1 (Figure 8c) and 0.98 for S2 (Figure 8d), with a slope of regression of 0.91 and 0.88, respectively. For all data,  $d_a$  was 0.94,  $C_{NS}$  was 0.85,  $MAE$  was  $35.6 \text{ W m}^{-2}$ , and  $RMSE$  was  $58.6 \text{ W m}^{-2}$ . Similar statistics have been reported in the scientific literature when the measured hourly dynamics of  $LE$  are compared to predictions from energy balance models [2,20,23,60,61]. For the S-W model, using all data similar statistics found,  $d_a$  was 0.92,  $C_{NS}$  was 0.80,  $MAE$  was  $39.3 \text{ W m}^{-2}$ , and  $RMSE$  was  $63.8 \text{ W m}^{-2}$ .

For both field campaigns, S2 (Figure 8b,d) shows a minimum variation relative to the 1:1 line, as compared with S1 (Figure 8a,c). These differences could be attributed to the different topographic aspects of each block. Due to the sun position, the soil water content between rows on site S1 was always lower than S2 and apparently the model cannot capture that effect without considering the slope/aspects. In this current version, the SEB-PW model does not account for the effect of slopes on the surface energy balance. However, for both sites and field campaigns, the datasets have a high correlation, and the line and results are reasonably well distributed.

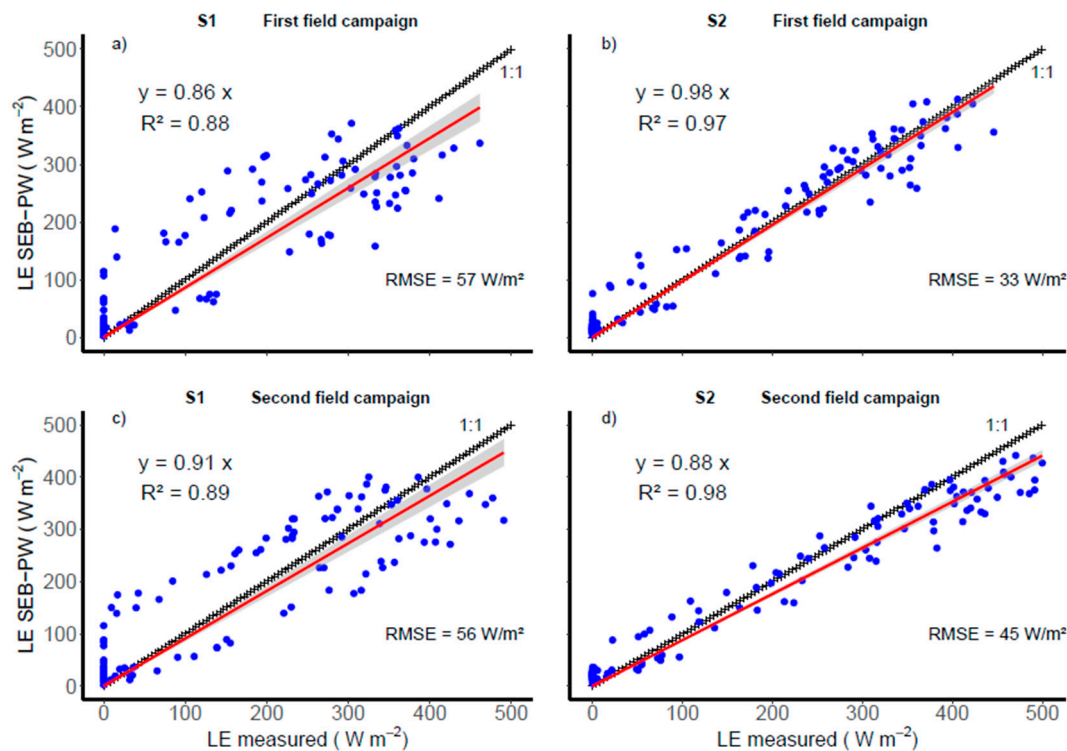


**Figure 8.** Measured versus modeled hourly latent heat flux from SR ( $LE_{measured}$ ) and SEB-PW ( $LE_{SEB-PW}$ ) for the first (June 15–20, a,b) and second (June 29–July 4, c,d) field campaigns.

Zhang et al. [61] also found that the slope of this regression was between 1.29–0.99 for a vineyard in an arid desert region, which indicated that the P-M model had good approximations regarding  $LE$ . Ortega-Farías et al. [20] found similar results at a Cabernet Sauvignon vineyard using the Shuttleworth and Wallace model under dry atmospheric conditions, with a  $MAE$  of  $22 \text{ W m}^{-2}$ . The same authors found that the maximum differences between the measured and estimated values were about  $67 \text{ W m}^{-2}$  and for high atmospheric demand. Poblete-Echeberría and Ortega-Farías [60] observed that  $LE$  estimated using a clumped model above a drip-irrigated Merlot vineyard had  $RMSE$  of  $36 \text{ W m}^{-2}$ .

The results show that the SEB-PW model for these field campaigns on the study vineyards had good agreement with the  $ET$  measurements, similar to other SEB models [2,20,23,69]. However, although the previous modeling efforts could discriminate crop transpiration from soil evaporation, they were not able to distinguish the evaporation from ground portions that were wetted by micro-irrigation versus that of non-wetted areas. This latter aspect represents the main novelty of the proposed SEB-PW model.

### Daily Soil Evaporation

During all trials,  $\lambda E_{soil}$  was higher on the first day after irrigation and decreased constantly during the next days. This occurred principally because the soil loses evaporable water easily and soil moisture tension increases after the irrigation days (Table 2). The soil evaporation weighed average immediately after irrigation ranged from 28% to 46% of the total  $ET$ . Similarly, Yunusa et al. [11] found that soil evaporation measured with MLs ranged between 50%–70% of the total  $ET$  during irrigation periods, whereas it was 8%–20% of the total  $ET$  during dry periods. Montoro et al. [70] also found similar values of  $\lambda E_{soil}$ , i.e., 11%–31% of the total  $ET$ , but also found higher  $\lambda E_{soil}$  values when large amounts of water were applied.

Figure 9 shows the correlation between the measured daily soil evaporation ( $E_s$ ) and the modeled evaporation from the SEB-PW model ( $E_{s \text{ SEB-PW}}$ ). The  $E_s$  measurements and SEB-PW predictions for all days for both S1 and S2 sites exhibited a deviation from the 1:1 line (Figure 9a), i.e., the SEB-PW model underestimated  $E_s$  values when  $E_s > 1.4 \text{ mm d}^{-1}$ . In other words, the model underestimated the daily soil evaporation, showing  $r^2$  of 0.95 and a slope of 0.97. However, a better correlation can be observed for  $E_s$  below  $1.3 \text{ mm d}^{-1}$ . The dynamics of the daily  $E_s$  indicated higher fluxes after irrigation (maximum of  $2.7 \text{ mm d}^{-1}$ ) and lower fluxes (about  $0.2$ – $0.6 \text{ mm d}^{-1}$ ), during the fourth day after irrigation. Zhao et al. [71] found a similar relation for the day after the irrigation and the following drying periods. Kerridge et al. [72] obtained daily  $E_s$  estimates, i.e., between  $0.6$  to  $2.5 \text{ mm d}^{-1}$ . Ding et al. [73] reported higher  $E_s$  after irrigation in the early growing seasons of maize when the canopy was small, while Kool et al. [74] reported that the  $E_s$  in a drip-irrigated vineyard was affected by wetting events, with  $E_s$  of  $0.35 \pm 0.06 \text{ mm d}^{-1}$  on days with irrigation,  $0.19 \pm 0.05 \text{ mm d}^{-1}$  on the day after, and  $0.1 \pm 0.04 \text{ mm d}^{-1}$  on the following days.

The differences between the soil evaporation from areas wetted ( $E_{sh}$ ) by the drip irrigation system (green-circles) and the soil evaporation from non-wetted areas ( $E_{ss}$ ) (black-circles) can be observed in Figure 9a. While  $E_{sh}$  reached a maximum value of  $2.4 \text{ mm d}^{-1}$ ,  $E_{ss}$  was normally less than  $0.5 \text{ mm d}^{-1}$  (21%). As predicted by the sensitivity analysis, the effect of  $E_{ss}$  on the total  $ET$  is very low (4%) when compared to  $E_{sh}$ . These relevant differences highlight the need to separate the wetted areas from those not wetted by the micro-irrigation system. When the SEB-PW (Figure 9a) and S-W (Figure 9b) models are compared to measurements of daily soil evaporation from micro-lysimeters, it is possible to observe that  $E_s$  from the SEB-PW model had a better agreement ( $r^2 = 0.95$ ) than the S-W model ( $r^2 = 0.81$ ). In addition,  $RMSE$  and  $MAE$  for daily  $E_s$  estimations from the S-W model (Figure 9b) compared with field measurements were  $0.55 \text{ mm d}^{-1}$  and  $0.46 \text{ mm d}^{-1}$ , respectively; better results can be observed with the SEB-PW model (Figure 9a). In other words, better agreement can be found when wetted and non-wetted areas are considered in the surface energy balance.

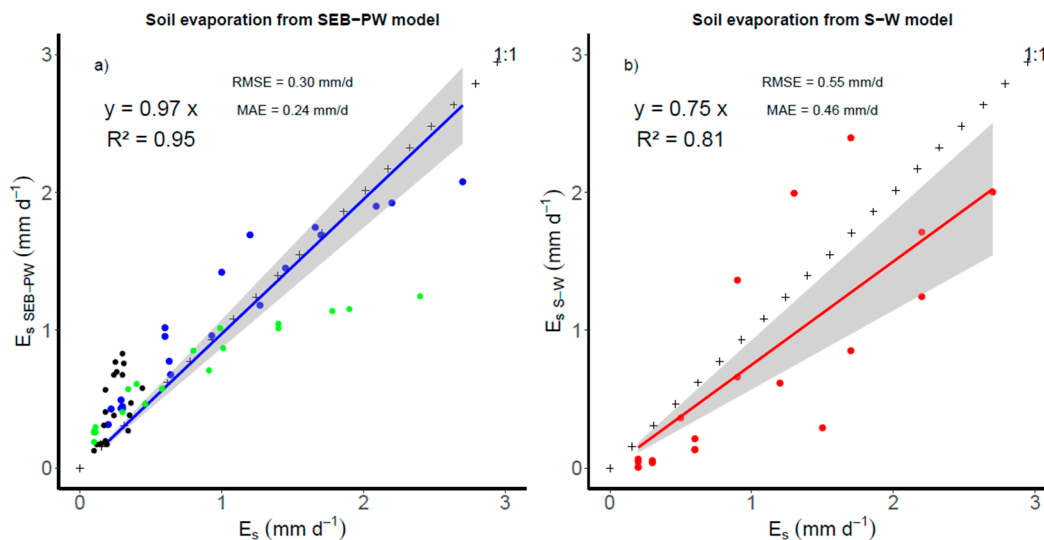


**Figure 9.** Comparison of the soil evaporation from microlysimeters ( $E_s$ ) versus soil evaporation modeled by the SEB-PW ( $E_{s\text{ SEB-PW}}$ ) and S-W ( $E_{s\text{ S-W}}$ ) models (a,b, respectively).  $E_{ss}$  is represented by black circles;  $E_{sh}$  is represented by green circles.

Figure 10 summarizes the relation between the daily  $ET_c$  by the SEB-PW model and  $ET_c$  by the SR method (Figure 10a), and the ratio of soil evaporation on  $ET$  ( $E_{ratio}$ ) by the SEB-PW model and obtained by micro-lysimeter and the SR method (Figure 10b). The  $P$ ,  $P_w$ , and  $LAI$  utilized can be seen in the Table A2 (Appendix A). As seen, the weighted soil evaporation, estimated by the SEB-PW model, reached maximum values (June 29) of 1.7 and 2.1  $\text{mm d}^{-1}$  at S1 and S2, respectively, while on the same date, the evaporation measured with MLs were  $1.7 \pm 0.04$  and  $2.7 \pm 0.02$   $\text{mm d}^{-1}$ , respectively. Similar standard deviations ( $\pm 0.06$   $\text{mm d}^{-1}$ ) for soil evaporation have been found in previous studies using the MLs technique [74]. Zhang et al. [75] measured soil evaporation between 0.1 and 3.59  $\text{mm d}^{-1}$ , with an average of 1.12  $\text{mm d}^{-1}$ , in a micro-irrigated vineyard with MLs. As expected, the measured  $E_{ratio}$  were higher the first day after irrigation for both periods, with 0.28 and 0.35 of  $ET$  at S1 and 0.46 and 0.45 of  $ET$  at S2, while lower values were found on the fifth day after irrigation, with an average of 0.05 for both periods and sites. The modeled soil evaporation ratio was also higher the first day after irrigation for both periods, with 0.35 and 0.38 of  $ET$  at S1 and 0.41 and 0.42 of  $ET$  at S2, while lower values were simulated for the fifth day after irrigation, with an average of 0.09 for both periods and sites. These results are comparable with other studies previously conducted, in which  $E_{ratio}$  varied from less than 0.10 in a vineyard in Southern Israel to 0.70 in a Chardonnay vineyard in Texas, US [76,77]. Montoro et al. [70] found that  $E_{ratio}$  ranged between 0.26–0.31 on days with a similar canopy cover and irrigation in a vineyard during the 2011–2014 seasons. Fandiño et al. [78] reported that  $E_{ratio}$  were 0.08–0.15, while Cancela et al. [79] observed  $E_{ratio}$  of 0.27 under drip-irrigation. For sparse vegetation stands, such as vineyards, soil evaporation may represent a significant fraction of the total  $ET$  due to the considerable ground area that is exposed to solar radiation and the atmosphere [80]. In general, the average soil evaporation, modeled and measured during the period of the first field campaign was 22% and 16% at S1 and 30% and 29% at S2, respectively. During the second field campaign, the average soil evaporation modeled and measured was 22% and 15% at S1 and 27% and 23% at S2, respectively. When compared with field measurements, daily  $E_s$  estimations from the SEB-PW model resulted in  $RMSE$ ,  $MAE$ ,  $C_{NS}$ , and  $d_a$  of 0.30  $\text{mm d}^{-1}$ , 0.24  $\text{mm d}^{-1}$ , 0.87, and 0.94, respectively.

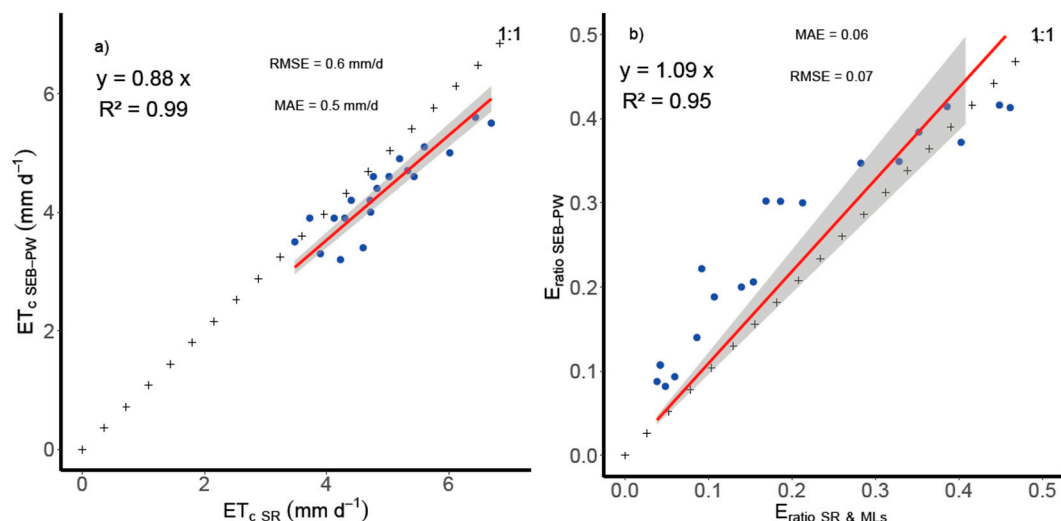


**Figure 10.** Daily evapotranspiration ( $ET_c$ ) and  $E_{ratio}$  ( $E_s/ET_c$ ) from the SEB-PW model compared with  $ET_c$  and  $E_{ratio}$  measured with the surface renewal method and micro-lysimeter (a,b, respectively).

#### 4. Conclusions

A modified SEB model (SEB-PW) was conceived for micro-irrigated orchard systems with partial ground wetting. Preliminary testing of SEB-PW was conducted on two drip-irrigated winegrape vineyards in Northern California for a range of shaded soil fractions ( $P$ ) and wet soil fractions ( $P_w$ ) during two five-day field campaigns in June–July 2018. The novel improvement of the SEB-PW model is the incorporation of fractional wetted soil in the surface energy balance algorithms. The SEB-PW model can be used to partition the total crop  $ET$  into crop transpiration, soil evaporation between rows (generally dry soil), and soil evaporation beneath the canopy (generally wetted soil by micro-irrigation). The sensitivity analysis showed that the calibration of  $r_c$  and soil resistances ( $r_i$ ) parameters are necessary in order to successfully apply the model for estimating evaporation and transpiration occurring in different crop and soils textures. The evaluation of model performance showed good agreement between modeled  $ET$  and  $E_s$  values and measurements conducted with surface renewal stations and MLs, respectively. The evaluation and modeling of  $E_{ratio}$  showed the relevance of this fraction (28%–46% of total  $ET$ ) after micro-irrigation events. When the SEB-PW model was compared with an existing model (S-W), better model performance was found when wetted and non-wetted areas are considered in the surface energy balance. The proposed SEB-PW model may be used to estimate the effect and magnitude of soil evaporation from wet and dry areas, alongside the total crop  $ET$ . As such, the model can better inform water balance studies to optimize micro-irrigation management practices. Further evaluation is needed to test the model in other partially wetted orchards and to test the model performance during all growing seasons and for longer periods.

**Author Contributions:** Conceptualization, C.S., O.L. and E.H.; Formal analysis, C.S., O.L., L.W., K.S., G.M., R.S. and D.Z.; Funding acquisition, O.L. and D.Z.; Investigation, C.S., O.L., E.H., R.S. and D.Z.; Methodology, C.S., O.L. and D.Z.; Project administration, D.Z.; Supervision, O.L., E.H. and D.Z.; Validation, C.S.; Visualization, C.S.; Writing—original draft, C.S., O.L. and D.Z.; Writing—review & editing, M.L.M., L.W., K.S., G.M. and E.H..

**Funding:** The research leading to this report was supported by the National Commission for Scientific and Technological Research (CONICYT) through CONICYT-PCHA/National Doctorate/2015-21150829, the project, CONICYT/FONDAP/15130015: Water Research Center for Agriculture and Mining (CRHIAM).

**Acknowledgments:** The authors thank the project, CONICYT/FONDAP/15130015: Water Research Center for Agriculture and Mining (CRHIAM), CONICYT-PCHA/National Doctorate/2015-21150829, and the Department of Water Resources at Universidad de Concepción. A special acknowledge to D. Zaccaria and the Department of Land, Air, and Water Resources of the University of California Davis.

**Conflicts of Interest:** The authors declare no conflict of interest.

**Appendix A. Mathematical Treatment and Additional Information**

For Equations (6) and (8):

$$r'_A = \frac{(r_{ss}+r_2) \cdot (r_{sh}+r_2)}{r_{sh} \cdot (1-P_w) + r_{ss} \cdot (P_w) + r_2}$$

$$r'_B = \frac{(r_{2ss}+r_{2b}) \cdot (r_{2sh}+r_{2b})}{r_{2sh} \cdot (1-P_w) + r_{2ss} \cdot (P_w) + r_{2b}}$$

For Equation (10)

$$X' = [R_{nC} \cdot \Delta \cdot r_1 \cdot A' + R_{nDC} \cdot \Delta \cdot r_2 \cdot r_L \cdot B'] \cdot P + [R_{ne} \cdot \Delta \cdot r_{2b} \cdot r_{2L} \cdot C'] \cdot (1 - P)$$

$$Y' = [A' + (r_{us} + r_{uh} + r_L + r_2) \cdot B'] \cdot P + [(r_{2us} + r_{2uh} + r_{2L} + r_{2b}) \cdot C'] \cdot (1 - P)$$

$$Z' = [\Delta \cdot (r_{us} + r_{uh} + r_2) \cdot B'] \cdot P + [\Delta \cdot (r_{2us} + r_{2uh} + r_{2b}) \cdot C'] \cdot (1 - P)$$

where:

$$A' = \frac{1}{\gamma \cdot (r_1 + r_c) + r_1 \cdot \Delta}$$

$$B' = \frac{1}{r_L \cdot \Delta \cdot (r_{us} + r_{uh} + r_2) + \gamma \cdot r'_A \cdot (r_{us} + r_{uh} + r_L + r_2)}$$

$$C' = \frac{1}{r_{2L} \cdot \Delta \cdot (r_{2us} + r_{2uh} + r_{2b}) + \gamma \cdot r'_B \cdot (r_{2us} + r_{2uh} + r_{2L} + r_{2b})}$$

For Equation (11):

$$J' = R_{nC} \cdot \gamma \cdot (r_1 + r_c) \cdot A' \cdot P + R_{nDC} \cdot D' \cdot P + R_{ne} \cdot E' \cdot (1 - P)$$

$$M' = A' \cdot P + F' \cdot P + G' \cdot (1 - P)$$

$$N' = \Delta \cdot H' \cdot P + \Delta \cdot I' \cdot (1 - P)$$

where:

$$D' = 1 - r_2 \cdot \varepsilon \cdot (r_L \cdot \Delta + \gamma \cdot r'_A)$$

$$E' = 1 - r_{2b} \cdot \mu \cdot (r_{2L} \cdot \Delta + \gamma \cdot r'_B)$$

$$F' = (r_{us} + r_{uh} + r_L + r_2) \cdot \varepsilon \cdot \left( \frac{r_L \cdot \Delta + \gamma \cdot r'_A}{r_L \cdot \Delta} \right) - \frac{1}{r_L \cdot \Delta}$$

$$G' = (r_{2us} + r_{2uh} + r_{2L} + r_{2b}) \cdot \mu \cdot \left( \frac{r_{2L} \cdot \Delta + \gamma \cdot r'_B}{r_{2L} \cdot \Delta} \right) - \frac{1}{r_{2L} \cdot \Delta}$$

$$H' = (r_{us} + r_{uh} + r_2) \cdot \varepsilon \cdot \left( \frac{r_L \cdot \Delta + \gamma \cdot r'_A}{r_L \cdot \Delta} \right) - \frac{1}{r_L \cdot \Delta}$$

$$I' = (r_{2us} + r_{2uh} + r_{2b}) \cdot \mu \cdot \left( \frac{r_{2L} \cdot \Delta + \gamma \cdot r'_B}{r_{2L} \cdot \Delta} \right) - \frac{1}{r_{2L} \cdot \Delta}$$

**Table A1.** Typical half day conditions in a vineyard in the central valley of California for the sensitivity analysis.

Variable	Range Value	Unit
$R_n$	600	$W m^{-2}$
$T_a$	25–35	$^{\circ}C$
$RH$	30–70	%
$u$	1–3	$m s^{-1}$
$T_m$	16–25	$^{\circ}C$
$LAI_{max}$	4	$m^2 m^{-2}$
$L_t$	0.05	m
$L_m$	0.5	m
$C_{ext}$	0.4–0.8	Adimensional

Table A1. Cont.

Variable	Range Value	Unit
$R_s \text{ max}$	1000	$\text{W m}^{-2}$
$R_s$	700	$\text{W m}^{-2}$
$P$	0.5	Adimensional
$P_w$	0.3–0.7	Adimensional
$C_1, C_2 \text{ and } C_3$	4.2, 0.0025 and 350	Adimensional
$a \text{ and } b$	1.2 and 5.1	$\text{s m}^{-1}$ and adimensional
$VPD$	1.25–2.75	kPa

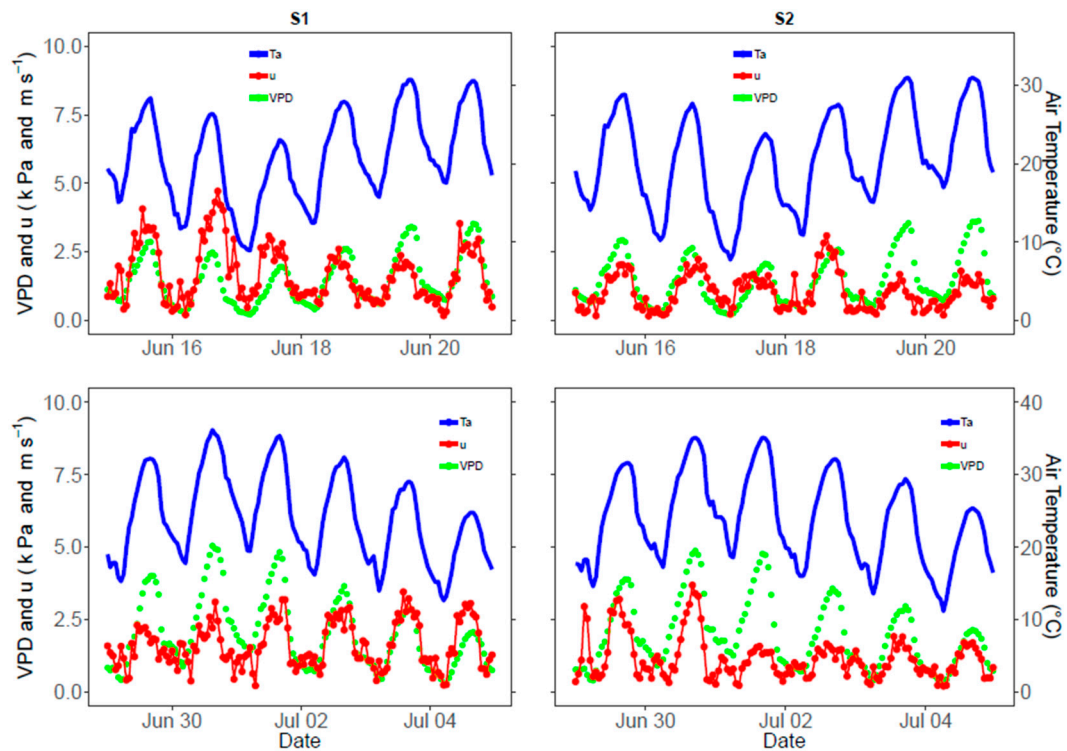


Figure A1. Environmental conditions during the 12-day period (first field campaign: 15 June–20 June and second field campaign: 29 June–4 July) at S1 and S2 for the vapor pressure deficit (VPD), wind speed ( $u$ ) and air temperature ( $T_a$ ).

Table A2. Fraction of the soil shadowed by plant canopy at solar noon ( $P$ ), wet soil fraction ( $P_w$ ) and leaf area index ( $LAI$ ).

Date	North Station			South Station		
	$P$ (%)	$P_w$ (%)	$LAI$ ( $\text{m}^2/\text{m}^2$ )	$P$ (%)	$P_w$ (%)	$LAI$ ( $\text{m}^2/\text{m}^2$ )
15-June		45			31	
16-June		41			26	
17-June	39	35	2.4	30	18	1.8
18-June		21			12	
19-June		10			10	
20-June		5			5	
29-June					50	
30-June		46			32	
1-July	41	37	2.5	31	22	1.8
2-July		21			10	
3-July		10			7	
4-July		5			5	

## References

1. Reitz, M.; Senay, G.B.; Sanford, W.E. Combining remote sensing and water-balance evapotranspiration estimates for the conterminous United States. *Remote Sens.* **2017**, *9*, 1181. [[CrossRef](#)]
2. Lagos, L.O.; Martin, D.L.; Verma, S.B.; Suyker, A.; Irmak, S. Surface energy balance model of transpiration from variable canopy cover and evaporation from residue-covered or bare-soil systems. *Irrig. Sci.* **2009**, *28*, 51–64. [[CrossRef](#)]
3. Wang, D.; Wang, L. Dynamics of evapotranspiration partitioning for apple trees of different ages in a semiarid region of northwest China. *Agric. Water Manag.* **2017**, *191*, 1–15. [[CrossRef](#)]
4. Burt, C.M.; Mutziger, A.J.; Allen, R.G.; Howell, T.A. Evaporation research: Review and interpretation. *J. Irrig. Drain. Eng.* **2005**, *131*, 37–58. [[CrossRef](#)]
5. Campbell, G.S.; Norman, J.M. *An Introduction to Environmental Biophysics*; Springer Science & Business Media: Berlin/Heidelberg, Germany, 2012.
6. Idso, S.B.; Reginato, R.J.; Jackson, R.D.; Kimball, B.A.; Nakayama, F.S. The three stages of drying of a field soil. *Soil Sci. Soc. Am. J.* **1974**, *38*, 831–837. [[CrossRef](#)]
7. Deol, P.; Heitman, J.; Amoozegar, A.; Ren, T.; Horton, R. Quantifying nonisothermal subsurface soil water evaporation. *Water Resour. Res.* **2012**, *48*, 1–11. [[CrossRef](#)]
8. Boast, C.W.; Robertson, T.M. A “Micro-Lysimeter” Method for Determining Evaporation from Bare Soil: Description and Laboratory Evaluation1. *Soil Sci. Soc. Am. J.* **1982**, *46*, 689. [[CrossRef](#)]
9. Evett, S.R.; Warrick, W.; Matthias, D. Wall Material and Capping Effects on Microlysimeter Temperatures and Evaporation. *Soil Sci. Soc. Am. J.* **1995**, *59*, 329. [[CrossRef](#)]
10. Todd, R.W.; Evett, S.R.; Howell, T.A.; Klocke, N.L. Soil temperature and water evaporation of small steel and plastic lysimeters replaced daily. *Soil Sci.* **2000**, *165*, 890–895. [[CrossRef](#)]
11. Yunusa, I.A.M.; Walker, R.R.; Lu, P. Evapotranspiration components from energy balance, sapflow and microlysimetry techniques for an irrigated vineyard in inland Australia. *Agric. For. Meteorol.* **2004**, *127*, 93–107. [[CrossRef](#)]
12. Penman, H.L. Natural evaporation from open water, bare soil and grass. *R. Soc. Lond. Ser. A Math. Phys. Sci.* **1948**, *193*, 120–145.
13. Monteith, J.L. Evaporation and environment. *Symp. Soc. Exp. Biol.* **1965**, *19*, 205–234. [[PubMed](#)]
14. Kjelgaard, J.F.; Stockle, C.O. Evaluating surface resistance for estimating Corn and Potato evapotranspiration with the Penman-Monteith model. *Trans. ASAE* **2001**, *44*, 797–805. [[CrossRef](#)]
15. Ortega-Farias, S.; Olioso, A.; Antonioletti, R.; Brisson, N. Evaluation of the Penman-Monteith model for estimating soybean evapotranspiration. *Irrig. Sci.* **2004**, *23*, 1–9. [[CrossRef](#)]
16. Shuttleworth, W.J. Towards one-step estimation of crop water requirements. *Trans. ASABE* **2006**, *49*, 925–935. [[CrossRef](#)]
17. Shuttleworth, W.J.; Wallace, J.S. Evaporation from sparse crops—an energy combination theory. *Q. J. R. Meteorol. Soc.* **1985**, *111*, 839–855. [[CrossRef](#)]
18. Farahani, H.J.; Ahuja, L.R. Evapotranspiration modeling of partial canopy/residue-covered fields. *Trans. ASAE* **1996**, *39*, 2051–2064. [[CrossRef](#)]
19. Stannard, D.I. Comparison of Penman-Monteith, Shuttleworth-Wallace, and modified Priestley-Taylor evapotranspiration models for wildland vegetation in semiarid rangeland. *Water Resour. Res.* **1993**, *29*, 1379–1392. [[CrossRef](#)]
20. Ortega-Farias, S.; Carrasco, M.; Olioso, A.; Acevedo, C.; Poblete, C. Latent heat flux over Cabernet Sauvignon vineyard using the Shuttleworth and Wallace model. *Irrig. Sci.* **2007**, *25*, 161–170. [[CrossRef](#)]
21. Zhao, P.; Li, S.; Li, F.; Du, T.; Tong, L.; Kang, S. Comparison of dual crop coefficient method and Shuttleworth-Wallace model in evapotranspiration partitioning in a vineyard of northwest China. *Agric. Water Manag.* **2015**, *160*, 41–56. [[CrossRef](#)]
22. Iritz, Z.; Lindroth, A.; Heikinheimo, M.; Grelle, A.; Kellner, E. Test of a modified Shuttleworth-Wallace estimate of boreal forest evaporation. *Agric. For. Meteorol.* **1999**, *98*, 605–619. [[CrossRef](#)]
23. Odhiambo, L.O.; Irmak, S. Performance of Extended Shuttleworth-Wallace Model for Estimating and Partitioning of Evapotranspiration in a Partial Residue-Covered Subsurface Drip-Irrigated Soybean Field. *Trans. ASABE* **2011**, *54*, 915–930. [[CrossRef](#)]

24. Ortega-Fari-as, S.; López-Olivari, R. Validation of a Two-Layer Model to Estimate Latent Heat Flux and Evapotranspiration in a Drip-Irrigated Olive Orchard. *Trans. ASABE* **2012**, *55*, 1169–1178. [[CrossRef](#)]
25. Choudhury, B.J.; Monteith, J.L. A four-layer model for the heat budget of homogeneous land surfaces. *Q. J. R. Meteorol. Soc.* **1988**, *114*, 373–398. [[CrossRef](#)]
26. Lagos, L.O.; Merino, G.; Martin, D.; Verma, S.; Suyker, A. Evapotranspiration of Partially Vegetated Surfaces. In *Evapotranspiration-Remote Sensing and Modeling*; InTech: London, UK, 2012.
27. Allen, R.G.; Asce, M.; Pereira, L.S.; Asce, M.; Smith, M.; Raes, D.; Wright, J.L.; Asce, M. FAO-56 Dual Crop Coefficient Method for Estimating Evaporation from Soil and Application Extensions. *J. Irrig. Drain. Eng.* **2005**, *131*, 2–13. [[CrossRef](#)]
28. Wilson, K.; Goldstein, A.; Falge, E.; Aubinet, M.; Baldocchi, D.; Berbigier, P.; Bernhofer, C.; Ceulemans, R.; Dolman, H.; Field, C.; et al. Energy balance closure at FLUXNET sites. *Agric. For. Meteorol.* **2002**, *113*, 223–243. [[CrossRef](#)]
29. Liu, S.; Mao, D.; Lu, L. Measurement and estimation of the aerodynamic resistance. *Hydrol. Earth Syst. Sci. Discuss.* **2006**, *3*, 681–705. [[CrossRef](#)]
30. Thom, A.S. 1972 Momentum, mass and heat exchange of vegetation. *Q. J. R. Meteorol. Soc.* **1972**, *98*, 124–134. [[CrossRef](#)]
31. Shuttleworth, W.J.; Gurney, R.J. The theoretical relationship between foliage temperature and canopy resistance in sparse crops. *Q. J. R. Meteorol. Soc.* **1990**, *116*, 497–519. [[CrossRef](#)]
32. Verma, S.B. Aerodynamic resistances to transfers of heat, mass and momentum. *Estim. Areal Evapotranspir.* **1989**, *177*, 13–20.
33. Wesely, M.L.; Hicks, B.B. Some factors that affect the deposition rates of sulfur dioxide and similar gases on vegetation. *J. Air Pollut. Control Assoc.* **1977**, *27*, 1110–1116. [[CrossRef](#)]
34. Lhomme, J.-P.; Chehbouni, A.; Monteny, B. Sensible heat flux-radiometric surface temperature relationship over sparse vegetation: Parameterizing B-1. *Bound. Layer Meteorol.* **2000**, *97*, 431–457. [[CrossRef](#)]
35. Runkle, B.R.K.; Wille, C.; Gažovič, M.; Wilmking, M.; Kutzbach, L. The surface energy balance and its drivers in a boreal peatland fen of northwestern Russia. *J. Hydrol.* **2014**, *511*, 359–373. [[CrossRef](#)]
36. Humphreys, E.R.; Lafleur, P.M.; Flanagan, L.B.; Hedstrom, N.; Syed, K.H.; Glenn, A.J.; Granger, R. Summer carbon dioxide and water vapor fluxes across a range of northern peatlands. *J. Geophys. Res. Biogeosci.* **2006**, *111*. [[CrossRef](#)]
37. Brenner, A.J.; Incoll, L.D. The effect of clumping and stomatal response on evaporation from sparsely vegetated shrublands. *Agric. For. Meteorol.* **1997**, *84*, 187–205. [[CrossRef](#)]
38. Brisson, N.; Itier, B.; L'Hotel, J.C.; Lorendeau, J.Y. Parameterisation of the Shuttleworth-Wallace model to estimate daily maximum transpiration for use in crop models. *Ecol. Model.* **1998**, *107*, 159–169. [[CrossRef](#)]
39. Lagos, L.O. A Modified Surface Energy Balance for Modeling Evapotranspiration and Canopy Resistance. Ph.D. Thesis, University of Nebraska, Lincoln, NE, USA, 2008.
40. Kato, T.; Kimura, R.; Kamichika, M. Estimation of evapotranspiration, transpiration ratio and water-use efficiency from a sparse canopy using a compartment model. *Agric. Water Manag.* **2004**, *65*, 173–191. [[CrossRef](#)]
41. Lund, M.R.; Soegaard, H. Modelling of evaporation in a sparse millet crop using a two-source model including sensible heat advection within the canopy. *J. Hydrol.* **2003**, *280*, 124–144. [[CrossRef](#)]
42. Camillo, P.J.; Gurney, R.J. A resistance parameter for bare-soil evaporation models. *Soil Sci.* **1986**, *141*, 95–105. [[CrossRef](#)]
43. Wunderlich, L.; Zaccaria, D.; Shackel, K.; Snyder, R. Investigating the Effect of Topography on Vine Water Use and Vine Stress. Available online: <http://www.asev.org/abstract/investigating-effect-topography-vine-water-use-and-vine-stress> (accessed on 10 December 2018).
44. California Soil Resource Lab. SSURG (Soil Survey Geographic). Available online: <https://casoilresource.lawr.ucdavis.edu/soilweb-apps> (accessed on 4 February 2019).
45. Burt, C.M. Rapid field evaluation of drip and microspray distribution uniformity. *Irrig. Drain. Syst.* **2004**, *18*, 275–297. [[CrossRef](#)]
46. Fulton, A.; Schwankl, L.; Lynn, K.; Lampinen, B.; Edstrom, J.; Prichard, T. Using EM and VERIS technology to assess land suitability for orchard and vineyard development. *Irrig. Sci.* **2011**, *29*, 497–512. [[CrossRef](#)]
47. Williams, L.E.; Ayars, J.E. Grapevine water use and the crop coefficient are linear functions of the shaded area measured beneath the canopy. *Agric. For. Meteorol.* **2005**, *132*, 201–211. [[CrossRef](#)]

48. Battany, M. Crop Coefficients-Paso Panel-San Luis Obispo County. Available online: [http://cesanluisobispo.ucanr.edu/Viticulture/Paso\\_Panel/](http://cesanluisobispo.ucanr.edu/Viticulture/Paso_Panel/) (accessed on 5 December 2018).
49. Kljun, N.; Calanca, P.; Rotach, M.W.; Schmid, H.P. A simple two-dimensional parameterisation for Flux Footprint Prediction (FFP). *Geosci. Model Dev.* **2015**, *8*, 3695–3713. [[CrossRef](#)]
50. Zitouna-Chebbi, R.; Prévot, L.; Jacob, F.; Mougou, R.; Voltz, M. Assessing the consistency of eddy covariance measurements under conditions of sloping topography within a hilly agricultural catchment. *Agric. For. Meteorol.* **2012**, *164*, 123–135. [[CrossRef](#)]
51. Hiller, R.; Zeeman, M.; Eugster, W. Eddy-covariance flux measurements in the complex terrain of an Alpine Valley in Switzerland. *Bound. Layer Meteorol.* **2008**, *127*, 449–467. [[CrossRef](#)]
52. Shapland, T.M.; Snyder, R.L.; Smart, D.R.; Williams, L.E. Estimation of actual evapotranspiration in winegrape vineyards located on hillside terrain using surface renewal analysis. *Irrig. Sci.* **2012**, *30*, 471–484. [[CrossRef](#)]
53. Marino, G.; Zaccaria, D.; Snyder, R.L.; Lagos, O.; Lampinen, B.D.; Ferguson, L.; Grattan, S.R.; Little, C.; Shapiro, K.; Maskey, M.L.; et al. Actual Evapotranspiration and Tree Performance of Mature Micro-Irrigated Pistachio Orchards Grown on Saline-Sodic Soils in the San Joaquin Valley of California. *Agriculture* **2019**, *9*, 76. [[CrossRef](#)]
54. Poblete-Echeverría, C.; Sepúlveda-Reyes, D.; Ortega-Farías, S. Effect of height and time lagon the estimation of sensible heat flux over a drip-irrigated vineyard using the surface renewal (SR) method across distinct phenological stages. *Agric. Water Manag.* **2014**, *141*, 74–83. [[CrossRef](#)]
55. Hu, Y.; Buttar, J.A.; Tanny, J.; Snyder, R.; Savage, M.J.; Lakhari, I.A. Surface Renewal Application for Estimating Evapotranspiration: A Review. *Adv. Meteorol.* **2018**, *2018*, 1–11. [[CrossRef](#)]
56. Haymann, N.; Lukyanov, V.; Tanny, J. Effects of variable fetch and footprint on surface renewal measurements of sensible and latent heat fluxes in cotton. *Agric. For. Meteorol.* **2019**, *268*, 63–73. [[CrossRef](#)]
57. Kisekka, I.; Oker, T.; Nguyen, G.; Aguilar, J.; Rogers, D. Revisiting precision mobile drip irrigation under limited water. *Irrig. Sci.* **2017**, *35*, 483–500. [[CrossRef](#)]
58. Villegas, J.C.; Breshears, D.D.; Zou, C.B.; Law, D.J. Ecohydrological controls of soil evaporation in deciduous drylands: How the hierarchical effects of litter, patch and vegetation mosaic cover interact with phenology and season. *J. Arid Environ.* **2010**, *74*, 595–602. [[CrossRef](#)]
59. Feng, H.; Chen, J.; Xu, Y. Effect of Sand Mulches of Different Particle Sizes on Soil Evaporation during the Freeze—Thaw Period. *Water* **2018**, *10*, 536. [[CrossRef](#)]
60. Poblete-Echeverría, C.; Ortega-Farías, S. Estimation of actual evapotranspiration for a drip-irrigated Merlot vineyard using a three-source model. *Irrig. Sci.* **2009**, *28*, 65–78. [[CrossRef](#)]
61. Zhang, B.; Kang, S.; Li, F.; Zhang, L. Comparison of three evapotranspiration models to Bowen ratio-energy balance method for a vineyard in an arid desert region of northwest China. *Agric. For. Meteorol.* **2008**, *148*, 1629–1640. [[CrossRef](#)]
62. Amer, K.H.; Hatfield, J.L. Canopy Resistance as Affected by Soil and Meteorological Factors in Potato. *Agron. J.* **2004**, *96*, 978–985. [[CrossRef](#)]
63. Williams, L.E.; Baeza, P. Relationships among ambient temperature and vapor pressure deficit and leaf and stem water potentials of fully irrigated, field-grown grapevines *Vitis vinifera* responses to light quality: Towards sustainable agricultural practices View project. *Am. J. Enol. Vitic.* **2007**, *58*, 173–181.
64. Moratiel, R.; Martínez-Cob, A. Evapotranspiration and crop coefficients of rice (*Oryza sativa* L.) under sprinkler irrigation in a semiarid climate determined by the surface renewal method. *Irrig. Sci.* **2013**, *31*, 411–422. [[CrossRef](#)]
65. Stoy, P.C.; Mauder, M.; Foken, T.; Marcolla, B.; Boegh, E.; Ibrom, A.; Arain, M.A.; Arneth, A.; Aurela, M.; Bernhofer, C.; et al. Agricultural and Forest Meteorology A data-driven analysis of energy balance closure across FLUXNET research sites: The role of landscape scale heterogeneity. *Agric. For. Meteorol.* **2013**, *171–172*, 137–152. [[CrossRef](#)]
66. Parry, C.K.; Kustas, W.P.; Knipper, K.R.; Anderson, M.C.; Alfieri, J.G.; Prueger, J.H.; Mcelrone, A.J. Comparison of vineyard evapotranspiration estimates from surface renewal using measured and modelled energy balance components in the GRAPEX project. *Irrig. Sci.* **2019**, *37*, 333–343. [[CrossRef](#)]
67. Legates, D.R.; McCabe, G.J. Evaluating the use of “goodness-of-fit” measures in hydrologic and hydroclimatic model validation. *Water Resour. Res.* **1999**, *35*, 233–241. [[CrossRef](#)]
68. Pushpalatha, R.; Perrin, C.; Le Moine, N.; Andréassian, V. A review of efficiency criteria suitable for evaluating low-flow simulations. *J. Hydrol.* **2012**, *420*, 171–182. [[CrossRef](#)]

69. Gavilán, P.; Berengena, J. Accuracy of the Bowen ratio-energy balance method for measuring latent heat flux in a semiarid advective environment. *Irrig. Sci.* **2007**, *25*, 127–140. [[CrossRef](#)]
70. Montoro, A.; Ma, F. Transpiration and evaporation of grapevine, two components related to irrigation strategy. *Agric. Water Manag.* **2016**, *177*, 193–200. [[CrossRef](#)]
71. Zhao, P.; Kang, S.; Li, S.; Ding, R.; Tong, L.; Du, T. Seasonal variations in vineyard ET partitioning and dual crop coefficients correlate with canopy development and surface soil moisture. *Agric. Water Manag.* **2018**, *197*, 19–33. [[CrossRef](#)]
72. Kerridge, B.L.; Hornbuckle, J.W.; Christen, E.W.; Faulkner, R.D. Using soil surface temperature to assess soil evaporation in a drip irrigated vineyard. *Agric. Water Manag.* **2013**, *116*, 128–141. [[CrossRef](#)]
73. Ding, R.; Kang, S.; Zhang, Y.; Hao, X.; Tong, L. Partitioning evapotranspiration into soil evaporation and transpiration using a modified dual crop coefficient model in irrigated maize field with ground-mulching. *Agric. Water Manag.* **2013**, *127*, 85–96. [[CrossRef](#)]
74. Kool, D.; Kustas, W.P.; Ben-Gal, A.; Lazarovitch, N.; Heitman, J.L.; Sauer, T.J.; Agam, N. Energy and evapotranspiration partitioning in a desert vineyard. *Agric. For. Meteorol.* **2016**. [[CrossRef](#)]
75. Zhang, Y.; Kang, S.; Ward, E.J.; Ding, R.; Zhang, X.; Zheng, R. Evapotranspiration components determined by sap flow and microlysimetry techniques of a vineyard in northwest China: Dynamics and influential factors. *Agric. Water Manag.* **2011**, *98*, 1207–1214. [[CrossRef](#)]
76. Netzer, Y.; Yao, C.; Shenker, M.; Schwartz, B.B.A. Water use and the development of seasonal crop coefficients for Superior Seedless grapevines trained to an open-gable trellis system. *Irrig. Sci.* **2009**, 109–120. [[CrossRef](#)]
77. Lascano, R.J.; Baumhardt, R.L.; Lipe, W.N. Measurement of Water Flow in Young Grapevines Using the Stem Heat Balance Method. *Am. J. Enol. Vitic.* **1992**, *43*, 159–165.
78. Fandiño, M.; Cancela, J.J.; Rey, B.J.; Martínez, E.M.; Rosa, R.G.; Pereira, L.S. Using the dual-Kc approach to model evapotranspiration of Albariño with consideration of active ground cover (*Vitis vinifera* L. cv. Albariño) with consideration of active ground cover. *Agric. Water Manag.* **2012**, *112*, 75–87. [[CrossRef](#)]
79. Cancela, J.J.; Fandiño, M.; Rey, B.J.; Martínez, E.M. Automatic irrigation system based on dual crop coefficient, soil and plant water status for *Vitis vinifera* (cv Godello and cv Mencia). *Agric. Water Manag.* **2015**, *151*, 52–63. [[CrossRef](#)]
80. Kool, D.; Agam, N.; Lazarovitch, N.; Heitman, J.L.; Sauer, T.J.; Ben-Gal, A. A review of approaches for evapotranspiration partitioning. *Agric. For. Meteorol.* **2014**, *184*, 56–70. [[CrossRef](#)]



© 2019 by the authors. Licensee MDPI, Basel, Switzerland. This article is an open access article distributed under the terms and conditions of the Creative Commons Attribution (CC BY) license (<http://creativecommons.org/licenses/by/4.0/>).